1   **Overlapping attentional networks yield divergent behavioral predictions across tasks:**

2   **Neuromarkers for diffuse and focused attention?**

3

4   Abbreviated title: Divergent predictions from attentional networks

5

6   Esther X.W. Wu[a,b], Gwenisha J. Liaw[b], Rui Zhe Goh[a], Tiffany T.Y. Chia[b], Alisia M.J. Chee[c],

7   Takashi Obana[a,b,e], Monica D. Rosenberg[f], B.T. Thomas Yeo[b,c,d,g,h], & Christopher L.

8   Asplund[a,b,d,e,g,h,*]

9

10   [a] Division of Social Sciences, Yale-NUS College, National University of Singapore, 16 College

11   Ave West, Singapore 138527

12   [b] N.1 Institute for Health, National University of Singapore, 28 Medical Drive, #05-COR,

13   Singapore 117456

14   [c] Department of Electrical and Computer Engineering, Faculty of Engineering, National

15   University of Singapore, Block E4, Level 5, Room 42, 4 Engineering Drive 3, Singapore 117583

16   [d] Clinical Imaging Research Centre, Yong Loo Lin School of Medicine, 14 Medical Drive, #B1-

17   01, Singapore 117599

18   [e] Department of Psychology, Faculty of Arts and Social Sciences, National University of

19   Singapore, 5 Arts Link, Singapore, 117570

20   [f] Department of Psychology, University of Chicago, Chicago IL, USA 60637

21   [g] Centre for Cognitive Neuroscience, Duke-NUS Medical School, 8 College Road, Singapore

22   169857

23   h Institute for Application of Learning Science and Educational Technology, National University

24   of Singapore, Singapore 119077

25

26   *To whom correspondence should be sent. Address: Yale-NUS College, 28 College Avenue

27   West #01-501, Singapore 138533. Tel: +65 6601 3327. Email: chris.asplund@yale-nus.edu.sg.

28

36

37   Number of pages for entire document (85), main text (52)

38   Number of figures (9), tables (3), multimedia (0) and 3D models (0)

39   Number of words for Abstract (250), Introduction (648), and Discussion (1497)

40   **Abstract**

41   Attention is a critical cognitive function, allowing humans to select, enhance, and sustain

42   focus on information of behavioral relevance. Attention contains dissociable neural and

43   psychological components. Nevertheless, some brain networks support multiple attentional

44   functions. Connectome-based Predictive Models (CPM), which associate individual differences

45   in task performance with functional connectivity patterns, provide a compelling example. A

46   sustained attention network model (saCPM) successfully predicted performance for selective

47   attention, inhibitory control, and reading recall tasks. Here we constructed a visual attentional

48   blink (VAB) model (vabCPM), comparing its performance predictions and network edges

49   associated with successful and unsuccessful behavior to the saCPM's. In the VAB, attention

50   devoted to a target often causes a subsequent item to be missed. Although frequently attributed to

51   attentional limitations, VAB deficits may attenuate when participants are distracted or deploy

52   attention diffusely. Participants (n=73; 24 males) underwent fMRI while performing the VAB

53   task and while resting. Outside the scanner, they completed other cognitive tasks over several

54   days. A vabCPM constructed from these data successfully predicted VAB performance.

55   Strikingly, the network edges that predicted better VAB performance (positive edges) predicted

56   *worse* selective and sustained attention performance, and vice versa. Predictions from the saCPM

57   mirrored these results, with the network's negative edges predicting better VAB performance.

58   Furthermore, the vabCPM's positive edges significantly overlapped with the saCPM's negative

59   edges, and vice versa. We conclude that these partially overlapping networks each have general

60   attentional functions. They may indicate an individual's propensity to diffusely deploy attention,

61   predicting better performance for some tasks and worse for others.

62

Significance statement

63

64   A longstanding question in psychology and neuroscience is whether we have general

65   capacities or domain-specific ones. For such general capacities, what is the common function?

66   Here we addressed these questions using the attentional blink (AB) task and neuroimaging.

67   Individuals searched for two items in a stream of distracting items; the second item was often

68   missed when it closely followed the first. How often the second item was missed varied across

69   individuals, which was reflected in attention networks. Curiously, the networks' pattern of

70   function that was good for the AB was bad for other tasks, and vice versa. We propose that these

71   networks may represent not a general attentional ability, but rather the tendency to attend in a

72   less focused manner.

Introduction

73

74   Attention is a critical cognitive function, allowing humans to select, enhance, and sustain

75   focus on information of behavioral relevance. Visual attention plays numerous roles in different

76   contexts, and it has been fractionated both behaviorally and neurally (Chun, Golomb, & Turk-

77   Browne, 2011; Desimone & Duncan, 1995; Egeth & Yantis, 1997). In addition to such separable

78   components, however, some brain networks support attentional processing across multiple

79   domains (Asplund, Todd, Snyder, & Marois, 2010; Corbetta & Shulman, 2002; Duncan, 2010;

80   Tamber-Rosenau, Dux, Tombu, Asplund, & Marois, 2013; Yeo, Krienen, et al., 2015). Recent

81   studies using Connectome-based Predictive Models (CPM) support this idea. In a CPM

82   approach, individual differences in behavioral performance are accounted for as a function of

83   whole-brain functional connectivity patterns, after which performance for novel individuals can

84   be predicted from fMRI data (Shen et al., 2017). Such predictions also apply across tasks. A

85   sustained attention network model (saCPM) (Rosenberg, Finn, et al., 2016) could predict

86   individual differences in performance for selective attention (Rosenberg, Hsu, Scheinost,

87   Constable, & Chun, 2018), inhibitory control (Fountain-Zaragoza, Samimy, Rosenberg, &

88   Prakash, 2019), and reading recall (Jangraw et al., 2018).

89   Here we constructed a CPM for the visual attentional blink (VAB), aiming to test

90   whether that model could predict performance on a variety of tasks and to compare its

91   predictions and network features to the saCPM's. In a VAB paradigm, participants search for

92   two items in a stream of distractors; they often fail to perceive the second item, but only when it

93   closely follows the first (200-500 ms) (Raymond, Shapiro, & Arnell, 1992). The VAB is

94   critically dependent on attention, as no deficit occurs when the first item is ignored. Individuals

95   differ in their VAB severity (rate of second item detection failures), and these differences are

5

96   typically large and stable (Dale, Dux, & Arnell, 2013). It is unclear, however, which cognitive

97   and neural factors underlie them. Numerous theoretical explanations have been proposed for the

98   VAB, including a temporary loss of control (Di Lollo, Kawahara, Shahab Ghorashi, & Enns,

99   2005) or bottleneck-like processing limitations (Chun & Potter, 1995). VAB magnitude also

100   correlates only weakly with most other attention tasks (Skogsberg et al., 2015).

101   Intriguingly, VAB performance sometimes improves when attention to its primary

102   detection task is reduced. Such reductions can be due to manipulation (Olivers & Nieuwenhuis,

103   2005, 2006) or dispositional factors (Dale & Arnell, 2010, 2015; Thomson, Ralph, Besner, &

104   Smilek, 2015), and are thought to cause more diffuse attentional deployment. In particular, mind-

105   wandering is associated with better VAB performance, though it has the opposite association for

106   many other attention tasks (Gonçalves et al., 2017; Hu, He, & Xu, 2012; Robertson, Manly,

107   Andrade, Baddeley, & Yiend, 1997; Smilek, Carriere, & Cheyne, 2010).

108   The VAB likely involves many factors (Dux & Marois, 2009), but which are reflected in

109   individual differences of brain network function? To address this question using a CPM

110   approach, we scanned 73 individuals while they performed the VAB task and while they rested.

111   Resting state data allowed us to assess whether any predictive functional architecture persisted

112   when participants were not engaged in attention-demanding tasks (Finn et al., 2015; Rosenberg,

113   Finn, et al., 2016; Yoo et al., 2017). Outside the scanner, the same individuals completed

114   cognitive tasks assessing sustained attention, selective attention, and fluid intelligence. We

115   constructed a visual attentional blink CPM (vabCPM), from which we could make and assess

116   predictions about the tasks. If attentional capacity predicts VAB performance, we would expect

117   *positive* associations between vabCPM predictions for behavior and observed performance in

118   other attention tasks. Conversely, if diffuse attentional tendencies predict VAB performance, we

119   might find significant *negative* associations between predicted and observed behavior for other

120   attention tasks. For external validation, we made and assessed predictions about our tasks,

121   including the VAB, using a sustained attention CPM (Rosenberg, Finn, et al., 2016). We then

122   investigated and compared the networks associated with each model to better understand their

123   relationship and potential psychological functions.

124

125   **Materials and Methods**

126   The present study included numerous tasks, with a primary focus on the visual attentional

127   blink (VAB). Additional tasks provided critical context and points of comparison for

128   understanding the individual differences in VAB performance and neural features. These

129   additional tasks included those related to goal-directed attention and fluid intelligence. Many of

130   these tasks are conceptually linked to the VAB (Dux & Marois, 2009), and many have also been

131   studied themselves using Connectome-based Predictive Modeling (Finn et al., 2015; Rosenberg,

132   Finn, et al., 2016; Rosenberg et al., 2018). To facilitate comparisons across these different tasks,

133   we re-coded all behavioral performance measures such that positive numbers indicated better

134   performance (e.g. higher accuracy or faster reaction times; see details below).

135   **Experimental design**

136   *Participants.* Eighty-two participants with self-reported normal or corrected-to-normal

137   vision and normal hearing were recruited from the National University of Singapore (NUS)

138   community. These individuals began a six-session study that included numerous behavioral and

139   neuroimaging components, a subset of which are reported and analyzed here. Eight participants

140   did not continue with the experiment after the first practice session (Session 0) and were

141   excluded from the following analyses. One participant who did not achieve a target

142   discrimination score of 75% in the main VAB task (Session 1) was also excluded. Thus, unless

143   otherwise stated, the following analyses included data from 73 participants (24 males) between

144   the ages of 19-30 (M = 22.25, SD = 1.84). All participants provided written informed consent in

145   accordance with a protocol approved by the NUS Institutional Review Board and received

146   monetary compensation.

147   *Stimulus presentation.* All sessions took place either inside the MR scanner or in the

148   laboratory over a span of 3 weeks (see Table 1-1 of Extended Data for complete and detailed

149   experimental protocol). Inside the scanner, stimuli were presented at a viewing distance of 91 cm

150   on a 32-inch LCD monitor (NordicNeuroLab, Bergen, Norway) with a screen refresh rate of 60

151   Hz, connected to a MacBook Air (OS 10.12.1) running PyschoPy (Peirce, 2007). Participants

152   made responses using an MR-compatible button box. In the laboratory, stimuli were presented at

153   a distance of 57 cm on a 22-inch LCD monitor (Samsung SyncMaster 2233) with a screen

154   refresh rate of 60 Hz using an NVIDIA Quadro FX 3450/4000 SD graphics card on Windows 7.

155   Participants' responses were captured on a standard computer keyboard. Auditory stimuli were

156   presented using PyschoPy (Peirce, 2007) binaurally through Creative headphones.

157   *Overview of task domains and specific tasks*. The tasks in this study all investigated

158   cognitive processing, primarily different forms of attention (Table 1). Each task is detailed

159   below, organized by task domain. The task domains included the Attentional Blink, Sustained

160   Attention, Selective Attention, and Fluid Intelligence.

161

162   Table 1. Schedule of tasks and data used in analysis. Participants were encouraged to take breaks

163   between the tasks to prevent fatigue. With the exception of the Raven's Progressive Matrices

164   test, each task was performed twice on non-successive days. Task domains and tasks were as

165   follows. Attentional Blink: Visual Attentional Blink (VAB) and Auditory Attentional Blink

166   (AAB). Sustained Attention: Visual Sustained Attention to Response Task (VSART), Auditory

167   Sustained Attention to Response Task (ASART), and Gradual-onset Continuous Performance

168   Task (GradCPT). Selective Attention: Attentional Network Task (ANT). Fluid Intelligence:

169   Raven's Progressive Matrices test (Raven's).

Session	Days after previous session	Task	Data used in analysis
0	0	VAB (practice)	Behavior
1	3 to 14	Resting state	FMRI
		VAB (in scanner)	FMRI, Behavior
		ANT, VSART	Behavior
2	1	AAB, GradCPT, ASART	Behavior
3	1	ANT, VSART, Raven's	Behavior
4	1	AAB, GradCPT, ASART	Behavior
5	1 to 10	VAB (in scanner)	Behavior

170

171

172   *Attentional Blink.* Participants completed a visual attentional blink (VAB) and an

173   auditory attentional blink (AAB) task. They were designed to be generally similar (Figure 1).

174   Both versions were built around target discrimination and a probe detection, with each item

175   embedded within a stream of distractors. Our main task of interest is the VAB, for which

176   neuroimaging data was collected concurrently. For the AAB and all other tasks, only behavioral

177   data were collected.

9

178

Visual Attentional Blink task
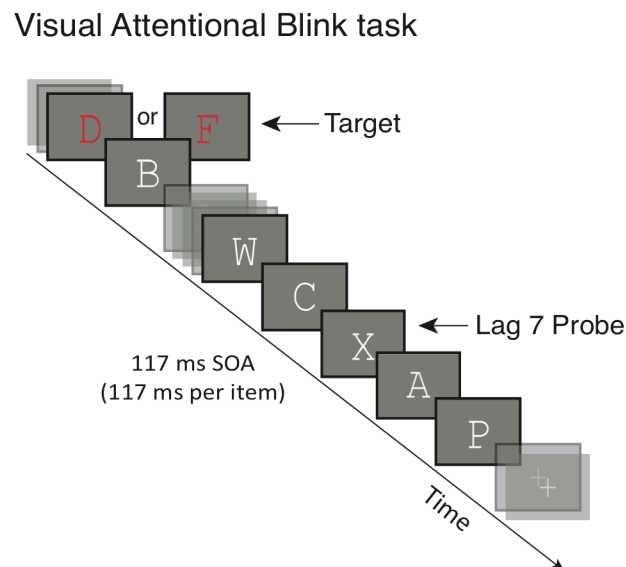
179

180   Figure 1. Experimental paradigm for the visual attentional blink (VAB) task. Participants

181   identified a target and then detected a probe within a stream of distractors, responding when

182   prompted at the conclusion of the stream. The target was a red letter, the probe was a white letter

183   X, and distractors were other white letters. The auditory attentional blink (AAB) task was

184   similar, save targets were complex tones, the probe was a high-pitched pure tone, and distractors

185   were other pure tones. SOA = stimulus onset asynchrony.

186

187   For the VAB, stimuli consisted of upper-case letters presented in Courier New Font on a

188   dark gray background (Figure 1). Targets were red letters D or F, whereas the probe was a white

189   letter X. Distractors were white letters save D, F, X, I, L, O, and Q. Targets and probes were

190   embedded within a rapid serial presentation stream, with no items repeated during each trial. The

191   stimulus onset asynchrony (SOA) between successive items in the 16-stimulus stream was 117

192   ms (no gap). A target appeared during every trial at serial position 3, 4, or 5, whereas the probe

193   appeared during 75% of trials. When present, the probe appeared at lags 1, 2, 3, 5, 7, or 9 relative

194   to the target, with the same number of trials per lag condition in each block. The first three lags

195   were expected to be within the AB window, whereas the last three were expected to be outside it.

196   In a small percentage of trials (14%), an irrelevant surprise stimulus (randomly selected from a

197   set of 24 grayscale male faces and 24 colorful objects) was presented at lags 2 or 6 relative to the

198   target. These surprise stimuli are not relevant to this current study; trials containing surprises

199   were excluded from the following analyses and are not reported further.

200   Each 6.25-second trial began with the presentation of a white fixation cross (0.8° x 0.8°)

201   for 500 ms, which became larger (1.0° x 1.0°) and turned yellow to signify that the rapid serial

202   visual presentation (RSVP) stream would begin in 750 ms. Participants searched this RSVP

203   stream (1867 ms) for the target and probe, which they then indicated by button box press after a

204   blank gap (233 ms) at the trial's conclusion. A maximum of 2.9 s was given for participants to

205   respond to both the target and probe response prompts. After this period, no further responses

206   were recorded and the white fixation cross returned until the start of the next trial. Failure to

207   respond was rare: No session had more than 0.16% no-target response trials or 0.64% no-probe

208   response trials averaged across participants, and no participant had more than 3.57% (target) or

209   4.17% (probe) no-response trials in any given session. The timing between each trial was

210   optimized for functional Magnetic Resonance Imaging (fMRI). As such, it followed an

211   exponential distribution with a range of 1.25-10 s and mean of 3.75 s. Each session contained six

212   blocks of 28 trials each, with the trials presented in a pseudorandom order. The 168 trials took

213   approximately 40 minutes to complete, including breaks. Before the main experimental blocks in

214   each session, each participant completed 3 practice blocks of 8 trials each. The first block

215   contained targets but no probes; the second block contained probes but no targets; and the third

216   block contained both.

217   For the AAB, targets were low-pitched or high-pitched complex tones comprised of five

218   log-related frequencies (794 to 1260 Hz, or 1349 to 2142 Hz), whereas the probe was a 4000 Hz

219   pure tone. Distractors were 19 pure tones of log-related frequencies ranging from 697 to 2911

220   Hz. Sound stimuli were adjusted to have equal mean absolute amplitudes, after which the probe

221   and distractor intensities were set to 45% and 30% of the target intensity (~70 dB). These values

222   were based on performance in Obana, Lim, & Asplund (under review) and additional pilot tests.

223   As in the visual task, a small percentage of auditory trials (14%) contained an irrelevant surprise

224   stimulus, randomly selected from a set of 24 sounds (including an alarm, a cough, and spoken

225   letters), presented at lags 2 or 6 relative to the target. Again, surprise trials were not analyzed

226   here. With the exception of a change in stimuli, trial structure was identical to the VAB.

227   Each 6.25-second trial began with a reminder of the target and probe sounds, which were

228   played for 110 ms each with a gap of 85 ms. After 750 ms, the rapid auditory stream (RAP)

229   began, through which participants searched for the target and probe. Similar to the visual task,

230   the identity of the target and the presence of the probe were indicated by keypress after a blank

231   gap (233 ms). Response prompts for the target and probe then appeared, with a maximum

232   allowed time of 2.9 s for both responses. The timing between each trial was fixed at 0.75 s.

233   Except for the blank gap and the response prompts, a white fixation cross (0.8° x 0.8°) was

234   shown on the screen throughout the block. Each session contained three blocks of 56 trials each,

235   with the trials presented in a pseudorandom order. The 168 trials took approximately 25 minutes

236   to complete, including breaks. Before the main experimental blocks in each session, each

237   participant completed 3 practice blocks of 8 trials each. The first block contained targets but no

238   probes; the second block contained probes but no targets; and the third block contained both.

239   Before beginning each practice and task block of the auditory task, participants could play the

240   target and probe sounds as many times as desired.

241   *Sustained attention.* To better understand VAB performance in relation to other forms of

242   attention and their neural underpinnings, we also ran three sustained attention tasks. These

243   paradigms included the visual and auditory versions of the Sustained Attention to Response Task

244   (SART; Robertson, Manly, Andrade, Baddeley, & Yiend, 1997), which we adapted from Seli,

245   Cheyne, Barton, & Smilek (2012), and the Gradual-Onset Continuous Performance Task

246   (GradCPT; Esterman, Noonan, Rosenberg, & DeGutis, 2013; Rosenberg, Noonan, DeGutis, &

247   Esterman, 2013). The SART has been frequently used to examine moment-to-moment

248   fluctuations of sustained attention, requiring participants to make continuous responses to most

249   stimuli but withhold responses to a few. However, due to its trial-based structure, which may

250   provide a short 'break' between trials and not tax attention sufficiently, the GradCPT was later

251   designed to present images that gradually transition from one to the next using a linear pixel-by-

252   pixel interpolation. The GradCPT has been shown to show reliable and large interindividual

253   variability amongst high-functioning young adults, such as those in our sample (Rosenberg,

254   Finn, et al., 2016; Rosenberg et al., 2013).

255   In the VSART, participants were presented single digits, one after another, in the center

256   of the display screen. They were asked to press the spacebar if they saw a number from 1 to 9,

257   but withhold their response if they saw the number 3. Each digit was presented for 250 ms,

258   followed by an encircled "x" mask for 900 ms. Digits were presented in Symbol font in white,

259   against a black background, at sizes 0.57^{o}, 1.03^{o}, 1.43^{o}, 1.89^{o}, 2.35^{o} of visual angle. The order of

260   the digits and their sizes were randomized. Participants completed 675 trials (~ 13.5 mins) in

261   each session.

262   For the ASART, stimuli consisted of spoken single numbers. As in the visual task,

263   participants were asked to press the spacebar when they heard the numbers 1 to 9, but to

264   withhold their response if they heard the number 3. The numbers were presented in random

265   order, each for 250 ms, following by a pink noise mask of 900 ms. Throughout the experiment,

266   participants maintained fixation on a cross in the middle of the display. Each session consisted of

267   675 trials (~13.5 mins).

268   The GradCPT (Rosenberg et al., 2013) consisted of images that gradually transitioned

269   from one to the next using a linear pixel-by-pixel interpolation (ISI = 800 ms). Images consisted

270   of 10 mountain and 10 city scenes, randomly presented with 10% and 90% probability,

271   respectively, without repeats in consecutive images. Participants were instructed to press the

272   spacebar when a city scene was presented, but to withhold their response when a mountain scene

273   was presented. To tax sustained attention sufficiently, the GradCPT was performed in a single

274   block over a relatively long duration (15 min).

275   *Selective attention.* To understand the AB's relationship to other selective attention tasks

276   and their neural underpinnings, we also employed the Attentional Network Task (ANT), by Fan,

277   McCandliss, Sommer, Raz, & Posner (2002). This paradigm was designed to test three separable

278   components of selective attention: alerting, orienting and executive control (Posner & Petersen,

279   1990) within a single experimental session. Stimuli consisted of 5 black lines (some with

280   arrowheads) arranged horizontally in a row, against a grey background. The target, always an

281   arrow in the center, was flanked on each side by (i) two arrows pointing in the same direction as

282   the target (congruent condition), (ii) two arrows pointing in the opposite direction from the target

283   (incongruent condition), or (iii) two black lines without arrowheads (neutral condition). Each line

284   or arrow measured 0.55° horizontally, and the space between two adjacent objects measured

14

285   0.06°. To trigger attention orienting, all stimuli were presented either 1.06° above or below a

286   central fixation cross. Participants were asked to keep their eyes fixated on the fixation cross and

287   respond whether the target was pointing right or left.

288   Each trial started with a central fixation cross (400 – 1600 ms), followed by a warning

289   cue (100 ms), a second central fixation cross (400 ms), and finally, the stimuli consisting of

290   target and flankers presented either above or below a central fixation cross. Target and flankers

291   were presented for 1700 ms, or until a response was made, whichever was shorter. A fixation

292   cross was then presented until the end of trial (4000 ms after the first fixation period). For the

293   warning cue, four types of cues were presented: (i) no cue (a central fixation cross, similar to that

294   presented during the first and second fixation period, was presented), (ii) a center cue (an asterisk

295   was presented in the center, thus alerting the participant to the impending stimuli presentation),

296   (iii) double cue (two asterisks were presented above and below a central fixation cross, at both

297   possible locations of the target), and (iv) a spatial cue (an asterisk was presented at the

298   impending location of the target). Participants completed 3 blocks of 96 trials (4 cue conditions x

299   2 target locations x 2 target directions x 2 repetitions), with trials presented in random order. The

300   entire task lasted about 30 min.

301   *Fluid intelligence*. As a final comparison domain for understanding VAB performance

302   and the associated neural underpinnings, we measured fluid intelligence. Participants completed

303   a shortened, nine-item version (Form A; Bilker et al., 2012) of the original 60-item Raven's

304   Standard Progressive Matrices (Raven, Raven, & Court, 1998). The task was completed on a

305   laboratory computer, and there were no response time limits. The task consists of pattern

306   matching questions designed to measure abstract reasoning skills, and it has been typically used

307   in clinical settings as a non-verbal test of fluid intelligence.

308   **Statistical analyses for behavioral data**

309   Participants had to meet a minimum target discrimination (letter D or F?) score of 75%

310   for the VAB and 60% for the AAB to be included in the final sample. As a result, 73 sets of data

311   were available for all tasks, with the exception of the AAB task (n=71). For the AAB, two

312   additional participants were excluded because their target discrimination performance did not

313   meet the minimum threshold in each session. For all behavioral comparisons, *p*-values were

314   based on two-tailed comparisons. We also did not correct any behavioral comparisons for

315   multiple corrections, as we wanted to find any normality violations and used the task correlations

316   to identify any relationships that might affect our CPM results.

317   The computation of each behavioral measure is detailed in the following sections, again

318   organized by task domain. To obtain stable behavioral metrics, we computed a 'best score' for

319   each task metric. When data was available across two different sessions, the final score was

320   averaged across both sessions. (When data was available only from a single session, the final

321   score set to that session's.) We assessed whether the distribution of 'best scores' for each metric

322   departed from normality using Jarque-Bera tests. As many normality violations were found, we

323   used Spearman correlations of the 'best scores' to compare each pair of tasks. For tasks with two

324   sessions, we also calculated test-retest reliability. Due to the aforementioned normality

325   violations, Spearman correlations were again used.

326   *Attentional blink.* The VAB and AAB deficits were calculated in the same way. For each

327   participant, we first computed the mean probe detection accuracy for each lag condition,

328   contingent upon correct identification of the target. Probe detection accuracy scores were then

329   averaged across short-lag (lags 1, 2, or 3) and long-lag (lags 5, 7, 9) conditions. The former

330   condition was expected to be within the attentional blink window, whereas the latter condition

16

331   was expected to be outside it. The AB deficit was computed by regressing out the long-lag scores

332   from the short-lag scores of each participant (short-lag scores ~ long-lag scores), and then saving

333   the residuals (MacLean & Arnell, 2012). Larger and positive values indicated smaller attentional

334   deficits, and thus better task performance. Note that simply subtracting the short-lag from the

335   long-lag scores yielded highly similar VAB deficit scores ($r(71) = .955$). Visual AB scores

336   (VABresid) were obtained from sessions 1 and 5, and the auditory AB scores (AABresid) were

337   obtained from sessions 2 and 4.

338   *Sustained attention.* D-prime values were computed for the VSART, ASART and

339   GradCPT, with larger values indicative of better performance in sustained attention. VSART

340   scores (VSARTdprime) were obtained from sessions 1 and 3, ASART scores (ASARTdprime)

341   were obtained from sessions 2 and 4, and GradCPT scores (GradCPTdprime) were obtained from

342   sessions 2 and 4.

343   *Selective attention.* To measure overall task performance in the ANT task, we computed

344   the mean error rate (ANTerr) across all trials and the intra-individual variability of RTs

345   (ANTrtvar) for each participant. Intra-individual RT variability was computed as the standard

346   deviation divided by mean of correct-trial RTs. Arguably, this metric is a more sensitive measure

347   of task performance than mean error rate (Rosenberg et al., 2018; Wojtowicz, Berrigan, & Fisk,

348   2012), with higher RT variability being linked to lower accuracy in ANT tasks (Adolfsdottir,

349   Sorensen, & Lundervold, 2008; Lundervold et al., 2011).

350   We also calculated metrics for each attentional network in the ANT, which putatively

351   reflect their efficiencies. To do so, we compared the RTs between different trial conditions for

352   each participant (Fan et al., 2002; Rosenberg et al., 2018). For the alerting network, efficiency

353   was computed by subtracting the mean RT of double-cue condition from the mean RT of the no-

17

354   cue condition (ANTaert). Larger values would indicate faster responses due to the cue and thus

355   better task performance. For the orienting network, efficiency was computed by subtracting the

356   mean RT of spatial-cue condition from the mean RT of the center-cue condition (ANToert), thus

357   larger positive values would also imply faster responses due to the cue and better task

358   performance. For the executive control network, efficiency was computed by subtracting the

359   mean RT of the congruent condition from the mean RT of the incongruent condition (ANTcert).

360   In this case, smaller values would imply less interference by the flanker arrows and better task

361   performance. For all computations of efficiency with RTs, only trials with correct responses

362   were included.

363   For easier comparisons with the other behavioral measures, we re-coded the raw values

364   of mean error (ANTerr), RT variability (ANTrtvar), and executive control efficiency (ANTcert),

365   multiplying them by -1 such that larger values would also imply better task performance. ANT

366   scores were obtained from sessions 1 and 3.

367   *Fluid intelligence.* Accuracy scores for the nine-item Raven's test (RavensAcc) were

368   computed for each participant, with higher scores implying better performance.

369

370   Table 2. Summary of behavioral metrics, including their task domain and a description of their

371   calculation. Raw values for ANTerr, ANTrtvar and ANTcert were re-coded such that larger

372   values indicated better task performance.

Task domain	Metric	Description
Attentional Blink	VABresid	Residuals from regressing out long-lag scores from short-lag scores.
	AABresid	
Sustained Attention	VSARTdprime	Dprime scores.

	ASARTdprime	
	GradCPTdprime	
	ANTerr	Mean error across all trials.
	ANTrtvar	SD/M of correct-trial RTs.
Selective Attention	ANTaert	Alerting network efficiency. No-cue RT minus double-cue RT.
	ANToert	Orienting network efficiency. Center-cue RT minus spatial-cue RT.
	ANTcert	Executive control network efficiency. Incongruent RT minus congruent RT.
Fluid Intelligence	RavensAcc	Mean accuracy.

373

374

MRI data collection and initial processing

Acquisition. MRI data were acquired at the Clinical Imaging Research Centre (Singapore) on a Siemens 3T MAGNETOM Prisma MRI scanner (Siemens, Erlangen, Germany) with a 32-channel head coil. Scanning parameters were adapted from the Human Connectome Project (HCP), and were chosen to ensure that full-brain coverage, including the cerebellum, was achieved for each participant. MRI data were acquired in Sessions 1 and 5 of the study, with the first session's data analyzed here. Each fMRI session started with a 5-min anatomical localizer scan, followed by four 8-min resting-state scans, six 5.25-min task-based (VAB task) scans, and a 5-min anatomical scan. During the resting-state runs, participants were asked to maintain fixation at a cross displayed in the center of the screen.

Imaging parameters. A 3D high-resolution (1 mm x 1 mm x 1 mm) T1-weighted MPRAGE pulse sequence was used to obtain whole-brain anatomical images for each participant, allowing for subsequent normalization to standard space. For each participant, 128 1-

19

388   mm thick contiguous sagittal slices (0.5 mm skip; 1 x 1 mm in-plane resolution) were acquired.

389   Other scanning parameters included a repetition time (TR) of 2300 ms, an effective echo time

390   (TE) of 2.22 ms, a flip angle of 8° and 260 mm field of view.

391   Functional MRI data were acquired with a multiband echoplanar imaging (MB-EPI;

392   CMRR release R2015; Feinberg et al., 2010; Moeller et al., 2010; Xu et al., 2013) sequence with

393   a MB acceleration factor of 8. 768 whole-brain images were obtained for each resting-state run

394   while 504 images were acquired for each task-based run. T2*-weighted images were acquired

395   using a TR of 625 ms, a TE of 33.2 ms and FA of 50°. Interleaved slices (imaging matrix = 64 x

396   64) were collected using a 220 mm field of view, with slice thickness at 2.50 mm (no gap). The

397   effective voxel size was thus 2.5 x 2.5 x 2.5 mm^3.

398   *Preprocessing.* Both task and localizer data were pre-processed using a previously

399   published pipeline for functional connectivity analyses (Fong et al., 2019; Kong et al., 2019)

400   publicly available at

401   https://github.com/ThomasYeoLab/CBIG/tree/master/stable_projects/preprocessing/CBIG_fMRI

402   _Preproc2016. Pre-processing steps across resting-state and task-based runs were the same,

403   except when mentioned otherwise. First, the initial four frames from each run were removed to

404   aid with BOLD signal stabilisation. Motion correction using FSL's MCFLIRT was then applied

405   such that runs with more than 50% of the frames exceeding a motion threshold were discarded to

406   ameliorate any contributions of head motion. The motion threshold was defined as frame

407   displacement (FD) > 75 and frame-to-frame intensity (DVARS) > 0.2 (Power, Barnes, Snyder,

408   Schlaggar, & Petersen, 2012). From this step, one task-based run (and no resting-state runs) was

409   removed from our data. FSL's bbregister function was used for intrasubject registration of the T1

410   anatomical images to the T2*-weighted images. The best run for each subject was used as the

411 registration file across all functional runs. Subsequently, motion parameters and their derivatives,

412 the global whole brain signal, the white matter signal, the cerebral spinal fluid signal and linear

413 trends were regressed out. Additionally, for task-based runs, we regressed out the haemodynamic

414 response signal aligned to trial onset times. Frames with excessive motion, identified earlier on,

415 were interpolated over (Power et al., 2014), and a temporal filter was applied to retain

416 frequencies between 0.009 and 0.08 Hz. The resulting BOLD signal was projected to fsaverage6

417 surface space and spatially smoothed with an isotropic Gaussian kernel of 6 mm (FWHM).

418   *Functional connectivity.* Functional connectivity was evaluated in fsaverage6 surface

419 space for 400 cortical regions (Schaefer et al., 2017) and in MNI152 volumetric space for 19

420 subcortical regions (including the brain stem, and the left and right hemispheres of the

421 accumbens area, amygdala, caudate, cerebellum, ventral diencephalon, hippocampus, pallidum,

422 putamen, and thalamus), with a total of 419 parcellations. For each run, the mean time course of

423 all the parcellations were correlated using Pearson's product moment correlation, resulting in a

424 419 (rows) x 419 (columns) correlation matrix, with (419 x 419 – 419) / 2 = 87,571 unique

425 values. Each cell in the correlation matrix represents a functional connection (edge) between a

426 pair of parcellations. Fisher r-to-z transformation was applied to increase normality (Van Dijk et

427 al., 2010). For each participant, Fisher-transformed matrices for all four resting-state scans and

428 all six task-based scans were averaged separately, forming two functional connectivity (FC)

429 matrices: resting-state FC (RSFC) and Visual Attentional Blink task FC (VABFC).

430   *Motion control.* To reduce the effects of motion on functional connectivity, we adapted

431 motion control procedures from Rosenberg et al. (2018) to remove edges that were correlated

432 with motion. For each participant, we measured the following five motion parameters from their

433 resting-state and task-based scans: (i) maximum displacement, (ii) maximum rotation, (iii) mean

434   frame-to-frame displacement, (iv) mean frame displacement (FD), and (v) mean frame-to-frame

435   intensity (DVARS). Spearman's rank correlation was computed across participants between each

436   edge in the FC matrix and each motion parameter. To be comparable with Rosenberg et al.

437   (2018), in which 72.7% of edges remained after controlling for motion, we removed edges where

438    $r > .275$ (two-tailed $p < .02$), leaving 69,617 edges, or 79.50% of the initial 87,571 edges. Edges

439   were removed from both VABFC and RSFC if they met the criteria for removal in either FC

440   matrix.

441   **General approach for Connectome-based Predictive Models (CPM)**

442   We adapted the Connectome-based Predictive Model (CPM) approach (Finn et al., 2015;

443   Rosenberg, Finn, et al., 2016; Rosenberg et al., 2018; Shen et al., 2017) to predict individual

444   differences in behavior from functional connectivity information (Figure 2). In the following

445   section, we first describe our CPM procedure and then summarize our different models. Data

446   from all 73 participants were included in these analyses (71 for models involving the AAB score,
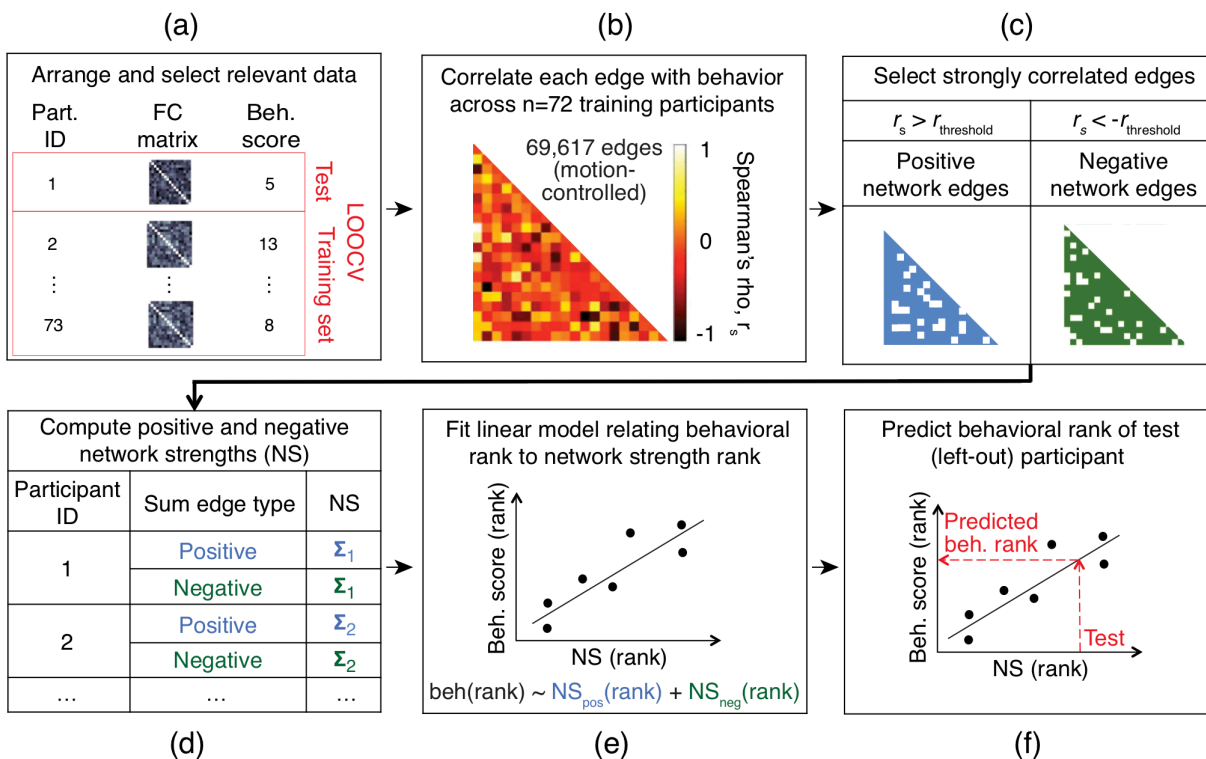
447   AABresid).

448

449

Figure 2. Procedure for Connectome-based Predictive Model (CPM) construction in the current

study (adapted from Shen et al., 2017). CPMs predict individual differences in behavior from

functional connectivity information. (a) Functional connectivity matrices and a behavioral score

of interest for each participant were calculated. One pair was held out of model construction for

each round of leave-one-out cross-validation (LOOCV) (Webb et al., 2011). (b) Functional

connectivity edges were correlated with behavior across participants. (c) Edges that correlated

most strongly, either positively or negatively, were selected. (d) Values from selected edges were

summed separately for positive and negative network edges, yielding two network strengths for

each participant. (e) A linear regression model relating (rank) network strengths to (rank)

behavioral scores was computed. (f) The model was tested on a novel, out-of-sample participant

(the individual left out in step (a)). After repeating steps a-f for each participant, the model was

evaluated by correlating the predicted behavioral scores with the actual scores.

462

463   *Model training.* We first selected an FC matrix (i.e., VABFC or RSFC) and a behavioral

464   score (e.g., VABresid). As part of the leave-one-out cross-validation procedure (Figure 2a), we

465   then set aside the data for one participant as test data and proceeded to train the model on the

466   remaining data (n = 72). To identify edges that most strongly correlated with behavior, we

467   computed Spearman's rank correlations between each unique edge in the FC matrix and the

468   behavioral score across 72 participants (Figure 2b), yielding 69,617 Spearman's rho values (r_s).

469   Edges positively related to behavior (positive network edges) were identified as those whose r_s

470   was greater than a pre-defined threshold, $r_{threshold}$, and edges negatively related to behavior

471   (negative network edges) were defined as those whose r_s was less than $-r_{threshold}$ (Figure 2c).

472   Next, we computed network strengths (NS) for each participant by summing up values in their

473   individual FC matrices across all positively and negatively correlated edges (Figure 2d),

474   resulting in 72 sets of positive NS and negative NS values. Subsequently, we converted the

475   positive NS, negative NS, and behavioral scores to rank space by ordering them according to

476   participants' values. Finally, we formulated a multiple linear regression model (Figure 2e) with

477   positive NS rank and negative NS rank as independent variables and behavioral rank as the

478   dependent variable i.e., Behavior (rank) $\sim$ NS$_{positive}$ (rank) + NS$_{negative}$ (rank).

479   *Model test.* We proceeded to predict the behavioral score (in rank space) of the test

480   participant (Figure 2f) by applying the training model to his/her FC matrix. Using the same

481   positive and negatively correlated edges identified from training, positive NS and negative NS

482   were first computed by summing up values in the FC matrix across the respective edges.

483   Following this step, positive and negative NS values of the test participant were ranked against

484   the relevant NS values of the training participants, and entered into the multiple linear regression

485   model to predict a behavioral rank.

486   *Model evaluation.* As part of the leave-one-out cross-validation procedure, the above

487   training and prediction steps were repeated on all participants ($N = 73$) such that each participant

488   was left out of training once, resulting in 73 sets of predicted behavioral ranks. To measure the

489   predictive power of the model, we obtained correlations between the predicted and observed

490   values, controlling for motion (Rosenberg et al., 2018). To this end, partial Spearman's rank

491   correlation was computed between predicted and observed behavioral ranks, with the motion

492   parameters (see section on Motion control) included as covariates. Where FC matrices were

493   different for training and test, motion parameters from both the resting-state and task-based scans

494   were included (i.e., ten covariates); where the same FC matrix was used, only motion parameters

495   from the relevant scan were included (i.e., five covariates). *P*-values for model evaluation were

496   left uncorrected, as most of the comparisons represented planned replications of previous work,

497   and the pattern of predictions across tasks was more informative than single model predictions.

498   For other neuroimaging-based statistical tests, we corrected for multiple comparisons, as detailed

499   in the respective Results sections (Functional connectivity and Network overlap).

500   **CPM model specification for data from the current study**

501   For each of the eleven behavioral scores (e.g., VABresid, AABresid, VSARTdprime,

502   etc.), we repeated the CPM procedure to train and test four different types of models. Two model

503   types (vabCPM model variants) were trained using FC information and behavioral responses

504   acquired from the main VAB task (i.e., VABFC and VABresid), and used to predict behavioral

505   performance of novel participants using either their VAB *task* (VABFC; Model type A), or their

506   *rest* (RSFC; Model type B) FC information. With these models, we sought to identify attentional

507   networks that were predictive of good VAB performance (positive network) and poor VAB

508   performance (negative network), and then to determine whether these networks generalized to

509   make similar predictions about other tasks. Two other model types (task-specific model variants)

510   were trained using task-specific behavioral data and either VAB *task* (VABFC; Model type C) or

511   *rest* (RSFC; Model type D) information. Behavioral performance was then predicted from the

512   same type of FC data that was used during training. With these models, we tested whether

513   predictive networks for each task could be predicted from FC data that was unrelated to that task;

514   any such predictive networks would be useful for identifying and comparing the edges that are

515   predictive of performance on a given task.

516   *Model type A (train on VABFC and behavioral data, predict with VABFC data).* For

517   training, the functional connectivity matrix VABFC and behavioral score VABresid were used to

518   select edges and form the linear model. For test, the training model was applied to the VABFC

519   matrix of the left-out participant. For evaluation, the predicted behavior from the leave-one-out

520   procedure was correlated with the behavioral score from a selected task.

521   *Model type B (train on VABFC and behavioral data, predict with RSFC data).* As in the

522   previous model, VABFC and VABresid were used for training, but for test, the training model

523   was applied to the RSFC matrix of the left-out participant. For evaluation, the predicted behavior

524   was correlated with the behavioral score from a selected task.

525   *Model type C (train and test on VABFC data).* During training, VABFC and the

526   behavioral score from a selected task were used to form the model. During test, the training

527   model was applied to VABFC of the left-out participant. For evaluation, the predicted behavior

528   was correlated with the observed score of the selected task.

529   *Model type D (train and test on RSFC data).* For training, the functional connectivity

530   matrix RSFC and the behavioral score from a selected task were used to form the model. For

531   test, the training model was applied to the RSFC of the left-out participant. During evaluation,

532   the predicted behavior was correlated with the observed score of the selected task.

533   *Controls.* For the primary analyses in the study, we implemented the CPM procedure

534   using edge selection cutoffs ($r_{threshold}$ = .232, p = .05) previously used in Rosenberg et al. (2018).

535   As an exploratory control, we also investigated whether our predictions were reasonably stable

536   across edge selection cutoff values. To do so, we repeated the leave-one-out cross-validation

537   procedure with $r_{threshold}$ ranging from .005 to .5, in steps of .005. Thus, in total, the CPM

538   procedure was repeated (11 behavior x 4 models x 101 edge selection thresholds) 4,444 times.

539   As p-values from LOOCV procedures can be biased, we verified the significance of our

540   models using permutation testing (Shen et al., 2017). A null distribution with 1000 iterations was

541   generated for each $r_{threshold}$. For each iteration, we randomly shuffled participants' behavioral

542   scores and repeated the prediction steps above. *P*-values (uncorrected for this exploratory

543   analysis) were computed as the proportion of permutation r_s with values greater than the

544   observed r_s.

545   **Sustained Attention CPM from Rosenberg et al. (2016)**

546   To compare our predictions and networks with another attention-related model, we

547   applied the Sustained Attention CPM (saCPM) (Rosenberg, Finn, et al., 2016) to our FC data.

548   The saCPM was constructed using FC data computed with 268 parcellations (Shen, Tokoglu,

549   Papademetris, & Constable, 2013). As our FC data was computed with 419 parcellations

550   (Schaefer et al., 2017), we transformed the Shen parcellations to Schaefer parcellations in

551   MNI152 space (91x109x91, 2mm voxels). For each Shen parcellation, we located the

27

552   corresponding Schaefer parcellation at a corresponding spatial location, excluding those that

553   accounted for less than 10% of the voxels in the Shen parcellation. Next, we mapped the saCPM

554   edges in the following way: if Shen parcellation A mapped to Schaefer parcellations 1, 2, and 3

555   and Shen parcellation C mapped to Schaefer parcellations 7 and 8, a functional connection

556   (edge) between Shen parcellations A and C would be mapped to Schaefer edges 1-7, 2-7, 3-7, 1-

557   8, 2-8, and 3-8. As before, edges that were removed previously due to motion were also removed

558   in the mapped saCPM edges.

559   We computed network strengths by taking the dot product between the saCPM edges and

560   our FC matrix (VABFC or RSFC), and entered the result into a linear model: Behavior ~

561    $NS_{positive} + NS_{negative}$. Note that these were motion-controlled FCs (69,617 edges), but during

562   evaluation, we did not implement partial correlation with motion parameters as co-variates,

563   following Rosenberg, Finn, et al. (2016). As the saCPM model was trained using FC data and

564   dprime scores acquired during the GradCPT task, predicted scores from the model were also

565   dprime scores. We evaluated the result of applying the saCPM to our FC data by computing

566   Spearman's rank correlation between the predicted scores and the scores from each of our

567   behavioral tasks.

568   **Network overlaps and edge locations**

569   *Degree of overlap.* To better understand the relationships across CPMs, we calculated the

570   percentage of network overlap for model pairs. First, for each model, we identified edges that

571   were common across all iterations of the leave-one-out procedure; we reasoned that these edges

572   were most representative of the model. For each pair of models, we expressed the number of

573   edges in common percentages of the number of edges in each model, and we then computed the

574   average of the two percentages. These percentages were calculated separately for positive-

575   positive, negative-negative, positive-negative, and negative-positive network overlaps.

576   To statistically assess whether the edges for each pair of models significantly overlapped,

577   we used the hypergeometric cumulative density function to determine the probability of drawing

578   up to x out of K possible items with n drawings without replacement, from a population of size M

579   (Rosenberg, Zhang, et al., 2016). The procedure was implemented with the hygecdf function in

580   (*MATLAB*, 2014), as $p = 1 - \text{hygecdf}(x, M, K, n)$, with x as the number of overlapping edges, M

581   as the total number of edges, K as the number of edges from one model, and n as the number of

582   edges from the other model. To control for multiple comparisons, FDR correction was applied

583   across the complete set of tests (Benjamini & Hochberg, 1995).

584   *Anatomical location of networks and overlaps*. To determine the anatomical locations of

585   network edges and the overlaps between the vabCPM and saCPM networks, we first grouped the

586   419 parcellations into network groups. The parcellations were matched to 17 network labels

587   (Yeo et al., 2011), from which they were aggregated into eight cortical groups (Yeo, Tandi, &

588   Chee, 2015) and a subcortical group. For each pair of network groups (e.g. Visual and Salience /

589   Ventral Attention), we computed the number of connections (network edges) between them. We

590   then reported this value as a percentage of the total number of possible connections between that

591   pair of network groups.

592

593   **Results**

594   In the sections below, we first report the behavioral results and the functional

595   connectivity matrices. We then present the behavioral predictions based on models derived from

596   the present dataset, followed by the behavioral predictions based on an external model (the

597   saCPM; Rosenberg et al., 2016). After comparing the pattern of predictions, we compare the

598   degree of overlap across the predictive networks. Finally, we examine the anatomical locations

599   of the overlaps between the vabCPM and saCPM networks.

600   **Behavioral performance**

601   We found a robust visual attentional blink (VAB) in each session, with substantially

602   impaired probe detection performance for the shorter lags (1, 2, 3) but not the longer lags (5, 7,

603   9) (Figure 3). For subsequent individual differences analyses, the VAB deficit was defined as

604   short-lag performance when controlling for long-lag performance (see Methods), a definition the

605   results supported. An AAB was also evidenced, though it was both smaller and less robust across
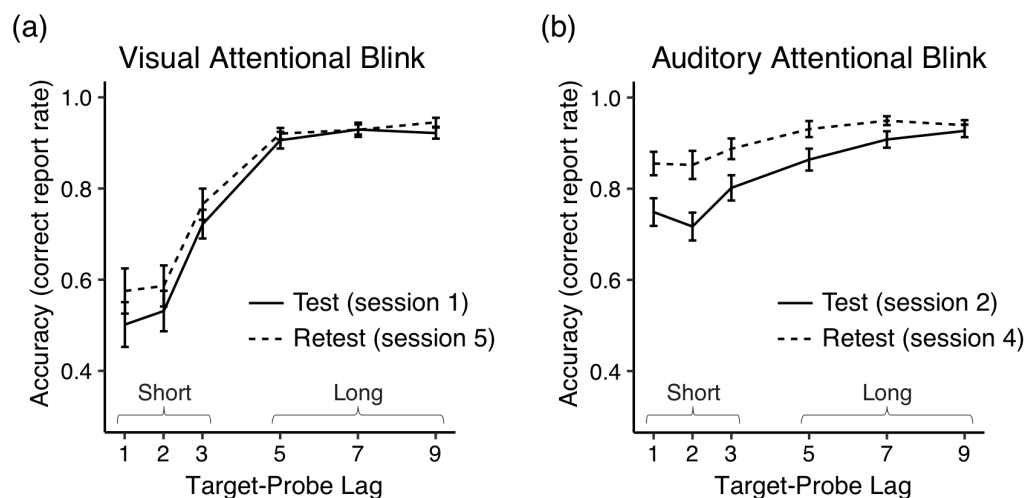
606   sessions.

607

608

609   Figure 3. Accuracy scores (probe hit rates) for the VAB and AAB. Note the substantial

610   impairment for the short target-probe lags (1, 2, and 3) in each session, especially for the VAB.

611   Error bars represent standard error of the mean (SEM).

612

613   Test-retest reliability was high for most metrics, and their ranges were reasonable (

614   Table 3). Jarque-Bera tests of normality revealed that several behavioral scores were not

615   normally-distributed (see relevant plots in Figure 4). Hence we adopted non-parametric

616   approaches in our subsequent analyses and models.

617

618   Table 3. Summary of behavioral data. Test-retest reliability (Spearman correlations across

619   sessions) was high for most metrics and significant for all (ps < .002). Jarque-Bera tests indicated

620   some significant departures from normality. Metrics are presented before re-coding. Metrics that

621   were subsequently reversed so that larger values would indicate better task performance are

622   marked with an asterisk (*). $N = 73$ for all metrics except AABresid ($N = 71$).

Task domain	Metric	Mean	SD	Range	Reliability (r_s)	Jarque-Bera (p)
Attentional Blink	VABresid	0.003	0.213	[-0.577, 0.356]	0.75	.126
	AABresid	0.001	0.118	[-0.412, 0.274]	0.38	.002
Sustained Attention	VSARTdprime	3.469	0.77	[1.016, 5.256]	0.54	.077
	ASARTdprime	3.187	0.795	[0.364, 5.127]	0.62	.004
	GradCPTdprime	2.844	0.655	[1.607, 4.359]	0.65	.144
Selective Attention	*ANTerr (% incorrect)	2.463	2.222	[0, 11.111]	0.66	.001
	*ANTrtvar (s)	0.147	0.035	[0.088, 0.24]	0.65	.058
	ANTaert (s)	0.074	0.022	[0.02, 0.138]	0.42	.447
	ANToert (s)	0.04	0.017	[0, 0.085]	0.36	.500
	*ANTcert (s)	0.129	0.03	[0.078, 0.207]	0.74	.100
Fluid Intelligence	RavensAcc (% correct)	82.5	15.15	[22.22, 100]	-	.001

623

31

624   To examine how behavioral performance was related across the various tasks, we

625   computed Spearman's rank correlations between each pair of behavioral scores (Figure 4).

626   Significant correlations were primarily found within a given attentional domain. The three

627   measures of Sustained Attention (VSARTdprime, ASARTdprime and GradCPTdprime) were

628   significantly correlated, as were the primary measures of Selective Attention (ANTerr and

629   ANTrtvar) and some of their component measures. Many of these metrics were significantly

630   correlated, positively and negatively, across the Sustained and Selective Attention task domains

631   as well. The negative correlations with the alerting (ANTaert) and orienting (ANToert) metrics

632   may be due to their reflecting stimulus-driven attentional control, as opposed to the goal-directed

633   control required for many other metrics. Attentional Blink (VABresid and AABresid) and Fluid

634   Intelligence (RavensAcc) metrics generally were not significantly correlated with other metrics.
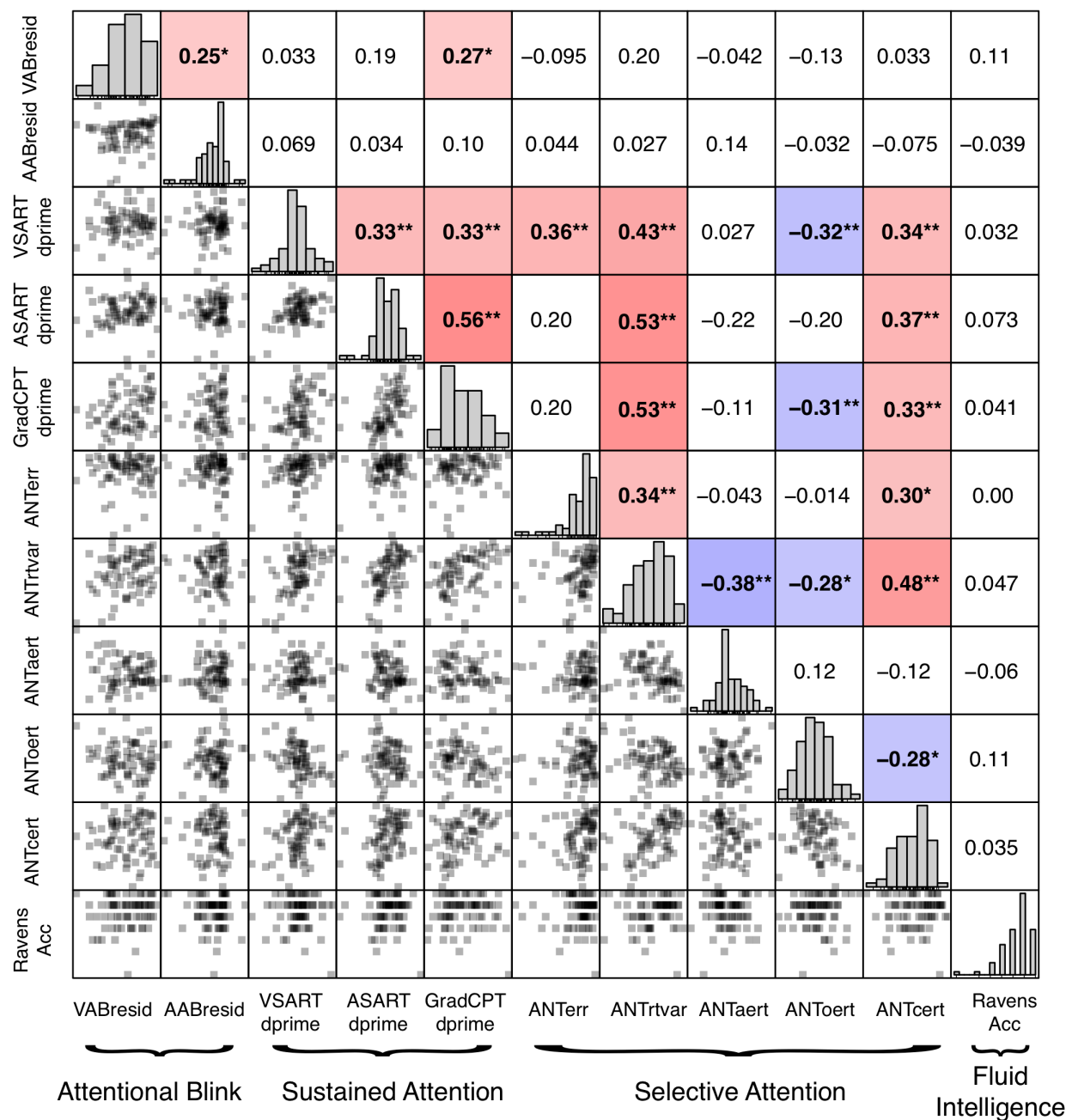
635

Figure 4. Behavioral score distributions and correlations. (Above diagonal) Spearman correlation coefficients for pairs of behavioral metrics. Most significant correlations were found within task domains, but some metrics correlated across the Sustained and Selective Attention domains. In contrast, Attentional Blink and Fluid Intelligence metrics largely did not correlate with other

641   metrics. Since the purpose of this analysis was to identify any behavioral relationships that might

642   explain subsequent CPM results, no correction for multiple comparisons was applied. *$p < .05$,

643   **$p < .01$. Red and blue shading indicates positive and negative relationships, respectively.

644   (Diagonal) Histograms of behavioral data. The behavioral data had been re-coded so that larger

645   values indicate better task performance for each measure. (Below diagonal) Scatterplots for each

646   pair of behavioral metrics.

647

648   **Functional connectivity matrices**

649   To assess and compare network connectivity during the VAB task and during rest, we

650   plotted group-averaged functional connectivity (FC) matrices (Figure 5). The 419 parcellations

651   from the FC matrices were matched to 17 network labels (Yeo et al., 2011), from which they

652   were aggregated into eight cortical groups (Yeo, Tandi, et al., 2015) and a subcortical group. FC

653   data from both the VAB task (VABFC; Figure 5a) and resting state (RSFC; Figure 5b) showed

654   similar connectivity patterns, with largely positive within-network correlations and mixed

655   directions for between-network correlations. The network correlation patterns were generally

656   similar to those observed in other data sets (Yeo et al., 2011; Yeo, Tandi, et al., 2015). Using

657   Network-based statistics to correct for multiple comparisons (Zalesky, Fornito, & Bullmore,

658   2010), we observed small differences between the two FC matrices, with many connections

659   linking the Salience/Ventral attention and the Dorsal attention networks (Figure 5c). Such

660   differences are consistent with the reported neural correlates of the attentional blink, which are in

661   frontal and parietal areas associated with the ventral and dorsal attention networks (Marois,

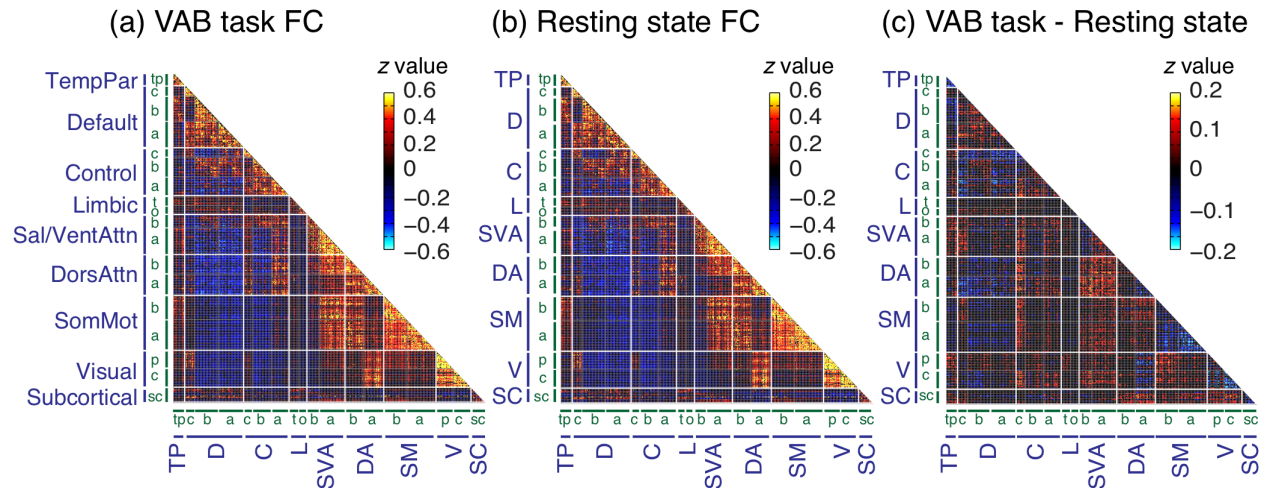662   Chun, & Gore, 2000; Marois & Ivanoff, 2005).

Figure 5. Functional connectivity (FC) matrices. Each edge was Fisher-transformed, and the resulting *z*-scores were averaged across participants. Edges found to correlate with motion were set to zero. (a) VAB task FC matrix (VABFC). (b) Resting-state FC matrix (RSFC). VABFC and RSFC patterns were similar to one another and to other data sets (Yeo et al., 2011; Yeo, Tandi, et al., 2015). (c) Difference FC matrix (VABFC - RSFC), showing edges that were significant at *p* = .05, corrected for multiple comparisons using network-based statistics. Differences between FC matrices were small, though they notably included connections linking the Salience/Ventral attention and the Dorsal attention networks. The 419 parcellations from the FC matrices were matched to 17 network labels (Yeo et al., 2011) (green labels), from which they were aggregated into eight cortical groups (Yeo, Tandi, et al., 2015) and a subcortical group (blue labels, spelled out in full in (a)). Subcortical regions include the brain stem, accumbens area, amygdala, caudate, cerebellum, ventral diencephalon, hippocampus, pallidum, putamen, and thalamus. For the green labels, letters represent the networks within the corresponding group, e.g., a(Default A), b(Default B), c(Default C), tp(TempPar), t(temporal pole in limbic region), o(orbital frontal cortex in limbic region), p(peripheral visual area), c(central visual area), and sc(subcortical).

Behavioral predictions from CPMs constructed using the present dataset

680

681   Models constructed from VAB functional connectivity and behavioral data (vabCPMs)

682   positively predicted VAB performance from task data (VABFC; Model type A) but not from

683   resting state data (RSFC; Model type B) (Figure 6a; corresponding values are tabulated in Figure

684   6-1 in the Extended Data). Task predictions were made in relative performance ranks (Spearman

685   correlations), so these predictions readily applied to other rank-order behavioral scores. When so

686   applied, we found that Fluid Intelligence performance could be positively predicted from both

687   task and rest FC data. Critically, the correlations between predicted and actual performance for

688   Sustained Attention metrics were *negative*, as were these correlations for Sustained Attention

689   tasks, albeit less consistently. Such results are counterintuitive, as all behavioral scores were re-

690   coded so that larger values indicated better performance. Furthermore, one might expect that

691   individuals whose network data predicted better performance on the VAB and Fluid Intelligence

692   tasks would perform worse on Sustained Attention and Selective Attention tasks. In reality,

693   however, VAB performance correlated insignificantly or weakly positively with other task

694   metrics, whereas Fluid Intelligence performance was not significantly correlated with any other

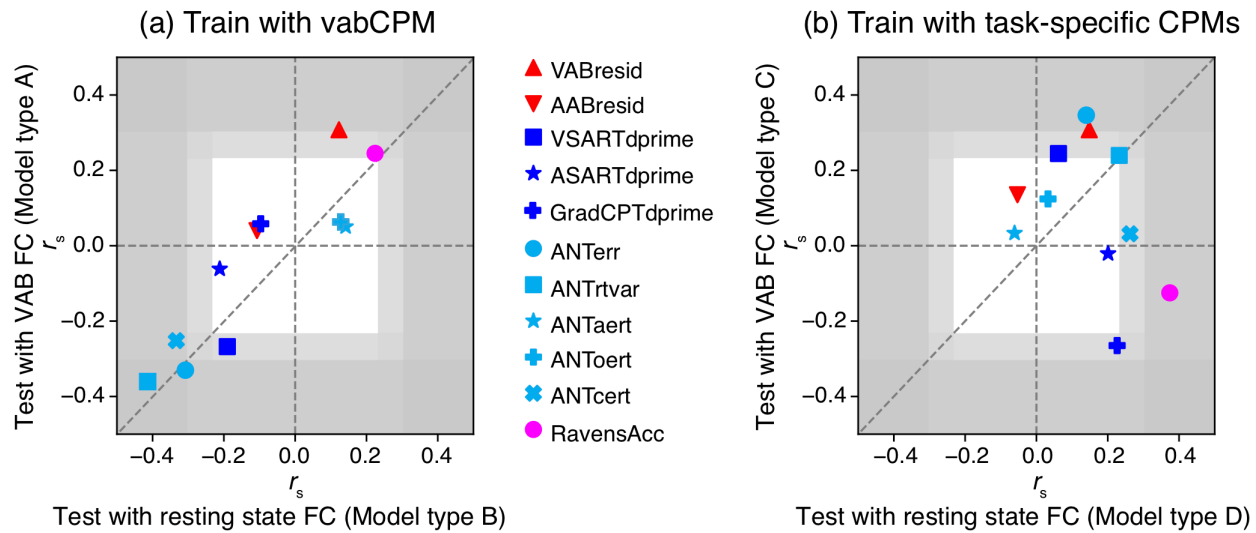695   tasks. We return to this intriguing result in the Discussion.

696

Figure 6. Behavioral predictions from CPMs. Each point represents a pair of Spearman's rank correlation coefficients (r_s) computed between observed and predicted behavioral scores for a given model type. (a) Predictions from vabCPMs, which were trained with VABFC and VABresid. Note the successful positive predictions for the VAB and Fluid Intelligence, but successful *negative* predictions for some Selective and Sustained Attention metrics. (b) Predictions from task-specific models. Many models could successfully predict behavioral performance, though results often varied greatly across the FC source. For both panels, the dark gray region indicates where r_s values are significant at the $p = .01$ level, and the lighter gray region indicates where r_s values are significant at the $p = .05$ level (uncorrected, with $d.f. = 71$). The r_s values and corresponding p-values are tabulated in Figure 6-1 in Extended Data. A standard edge selection threshold ($r_{\text{threshold}} = .232$, $p = .05$) was used for all models, though results were similar across a wide range of threshold values (Figure 6-2 and Figure 6-3 in Extended Data). Finally, as p-values from LOOCV procedures can be biased, we verified our results for the VAB using permutation testing; significance from this method and parametric approaches was consistent across edge selection thresholds (Figure 6-4 in in Extended Data).

714   Models built from task-specific behavioral data significantly predicted performance for

715   each of the task metrics predicted from the vabCPMs, although the results were less consistent

716   between VABFC-based (Model type C) and RSFC-based (Model type D) predictions (Figure 6b;

717   corresponding values are tabulated in Figure 6-1 in the Extended Data). Although it is possible

718   that the different predictions reflect different information in the two FC data sources (Figure 3),

719   it is unclear whether the differences are stable or simply reflect difficulty in building models

720   from fMRI data for which the behavioral data were collected separately. Indeed, CPMs

721   constructed from fMRI data collected during task performance and that task's behavioral scores

722   tend to be more robust (Rosenberg, Finn, et al., 2016; Rosenberg et al., 2018; Yoo et al., 2017).

723   Regardless, due to the same FC-behavior pair being used during both training and test,

724   significant negative predictions from the vabCPMs became positive, as expected (e.g.,

725   VSARTdprime, ANTerr, ANTrtvat and ANTcert).

726   To examine whether model predictions were sensitive to the number of edges selected

727   during CPM training, we explored how r_s changes as a function of edge selection thresholds. R_s

728   values were observed to be reasonably stable across edge selection thresholds, though more

729   variation was observed in task-specific models (Model types C and D) than in vabCPMs (Model

730   types A and B) (Figure 6-2 and Figure 6-3 in Extended Data). Additionally, as p-values from

731   LOOCV procedures can be biased, we verified our results for the VAB using permutation

732   testing; significance from this method and parametric approaches was consistent across edge

733   selection thresholds (Figure 6-4 in in Extended Data). Each of these issues may have contributed

734   to the unexpected negative predictions for the GradCPTdprime metric, an aspect of the results to

735   which we return below.

736   **Behavioral predictions from an external CPM (saCPM; Rosenberg et al., 2016).**

737   For external validation of our model predictions, we applied the Sustained Attention

738   CPM (saCPM) to our data. The saCPM was trained on fMRI and behavioral data from the

739   GradCPT, a sustained attention task (Rosenberg, Finn, et al., 2016). When applied to our data,

740   the saCPM predictions were virtually mirror images of our vabCPM predictions (Figure 7).

741   Specifically, whereas the vabCPM predicted VAB and Fluid Intelligence performance positively

742   and predicted Sustained Attention and Selective Attention performance negatively, the saCPM

743   predicted VAB and Fluid Intelligence performance *negatively* and predicted Sustained Attention

744   and Selective Attention performance *positively*.

745   With these findings, we also replicated the results from Rosenberg et al. (2018).

746   Specifically, the saCPM was able to predict the error rates (ANTerr), reaction time variability

747   (ANTrtvar), and conflict (ANTcert) metrics for novel individuals in the ANT task. Conversely,

748   we failed to replicate the significant predictions for GradCPTdprime in our data, contrary to

749   expectations. This replication failure is puzzling because the GradCPT behavioral data showed a

750   reasonable spread of scores and good test-retest reliability (Table 3), and the saCPM and

751   vabCPM did make significant predictions on other Sustained Attention metrics in our data set.

752   We are currently exploring our GradCPT task and results further in our laboratory.
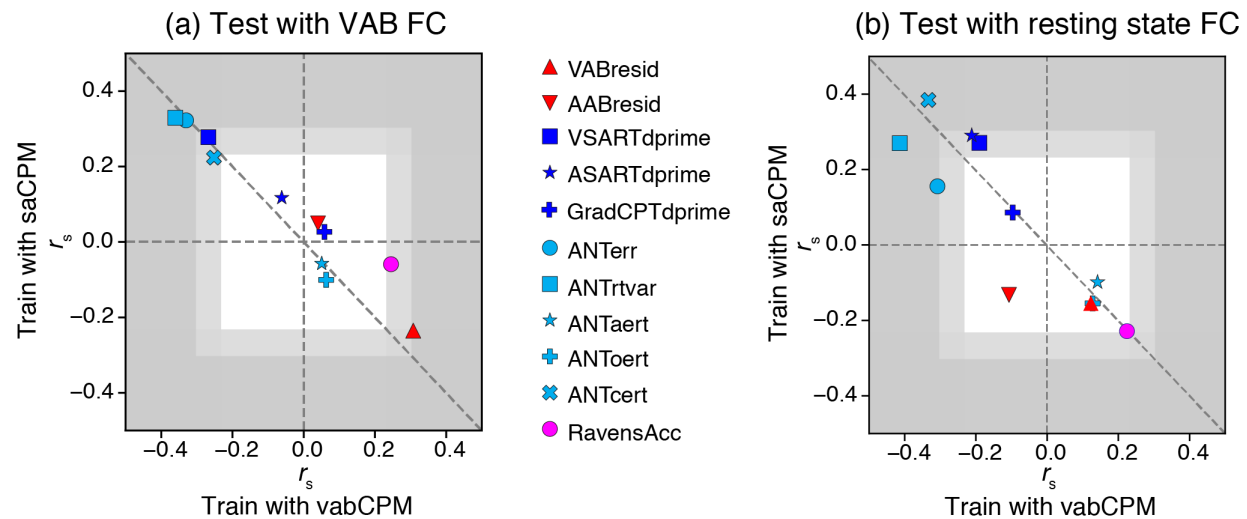
753

754

Figure 7. Comparison of predictions from the vabCPM and saCPM. Each point represents a pair

of Spearman's rank correlation coefficients (r_s) computed between observed and predicted

behavioral scores for a given model type. (a) Predictions from VABFC data. Note the saCPM's

successful positive predictions for some Selective and Sustained Attention metrics, with a

successful *negative* prediction for the VAB. As noted above, the prediction directions were

reversed for the vabCPM; indeed, the prediction points fall close to the diagonal. (b) Predictions

from RSFC data. The vabCPM and saCPM predictions went in opposite directions, and were

generally similar to the predictions from the VABFC. For both panels, the dark gray region

indicates where r_s values are significant at the $p = .01$ level, and the lighter gray region indicates

where r_s values are significant at the $p = .05$ level (uncorrected, with $d.f. = 71$). The edge

selection threshold ($r_{threshold}$) corresponded to $p = .05$ for all models. The r_s values and

corresponding p-values for the saCPM are tabulated in Figure 7-1 in the Extended Data. (See

Figure 6 for additional vabCPM details.)

Degree of overlap between predictive network pairs

40

770   To better understand how the underlying functional connectivity networks contributed to

771   the model predictions, we analyzed the extent to which edges were shared between pairs of

772   CPMs. For each pair, we calculated overlaps between positive network edges (those that

773   predicted better behavioral performance for the model's task), between negative network edges,

774   and across positive and negative network edges (Figure 8). The networks derived from the

775   vabCPM (VAB network) and saCPM (SA network) did not significantly overlap at similar

776   network edges (e.g. positive-positive; Figure 8a and 8b). Instead, they significantly overlapped

777   only at *opposing* network edges, the positive edges from one model and the negative edges from

778   the other (Figure 8c and 8d).

779   The overlaps between the VAB network and SA network accorded with their overlaps

780   with networks derived from other task-specific CPMs. VAB network edges tended to overlap

781   more with the opposing network edges of the Sustained and Selective Attention models (Figure

782   8c and 8d) as compared to their similar network edges (Figure 8a and 8b). In contrast, SA

783   network edges overlapped significantly with similar edges from each of the Sustained and

784   Selective Attention models, but with none of their opposing edges. Finally, although VAB and

785   Fluid Intelligence networks overlapped significantly only at similar network edges, SA network

786   edges did not significantly overlap with either similar or opposing Fluid Intelligence network

787   edges.

788   Taken together, the pattern of edge overlaps accords with the pattern of behavioral

789   predictions. The VAB and SA networks overlapped at opposing edges, and their predictions

790   were also negatively related (Figure 7). Predictions for individual metrics also aligned with

791   model overlaps. In general, when a metric's observed scores positively correlated with scores

792 predicted from the vabCPM or saCPM, that metric's CPM-derived network tended to overlap

793 with the VAB or SA network at similar network edges.
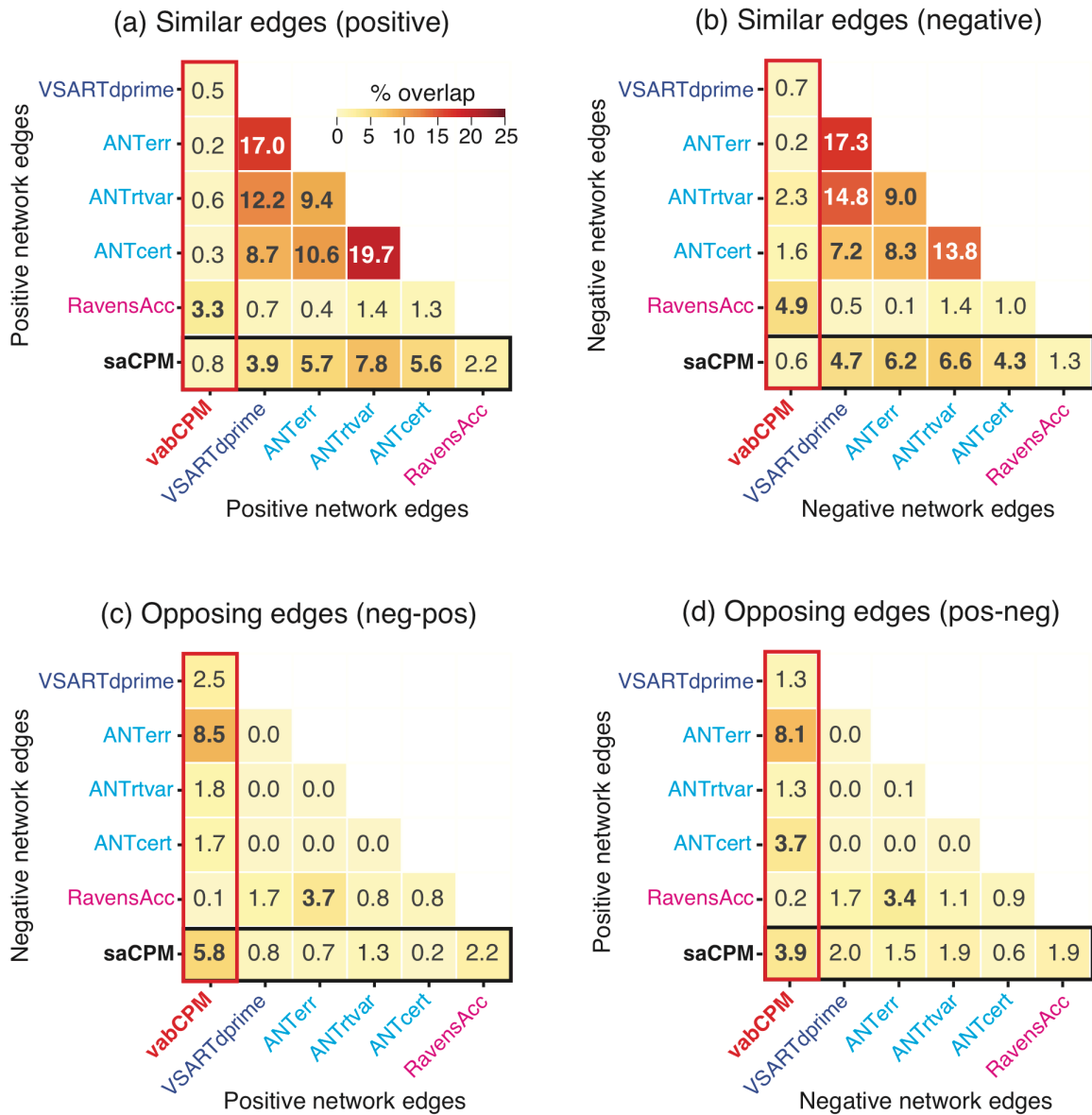
794

795
796 Figure 8. Percentage of edge overlap between networks from selected pairs of CPMs. Each task-

797 specific model was based on VABFC data (Model type C). Model pairs with statistically

798 significant overlap ($p < .05$, FDR corrected) are indicated in bold. Positive network edges

799 predicted better behavioral performance for their associated metric, whereas negative network

800   edges predicted worse behavioral performance. Overlap between *similar* network edges, (a)

801   positive-positive and (b) negative-negative. Sustained Attention (including the saCPM) and

802   Selective Attention models overlap primarily on similar edges, as do Fluid Intelligence and the

803   vabCPM. Overlap between *opposing* network edges, (c) negative-positive and (d) positive-

804   negative. The vabCPM network primarily overlaps with Sustained Attention (including the

805   saCPM) and Selective Attention on their opposing edges. Only task metrics that were

806   significantly predicted by vabCPMs using VABFC information are shown. The full set of

807   overlaps for all CPMs can be found in the Extended Data (Figure 8-1, 8-2, 8-3, and 8-4). Note

808   that the highest overlap value for any pairwise comparison, including each task metric predicted

809   from VABFC and RSFC, was 26.5%.

810

811   We also observed significant overlaps between similar network edges from Sustained and

812   Selective Attention models (Figure 8a and 8b). Similarly, Rosenberg and colleagues observed

813   substantial overlaps between a high attention (positive) network from the GradCPT task and

814   networks predicting high accuracy and low RT variability (better performance) in the ANT

815   (Rosenberg et al., 2018). Taken together, these results suggest that sustained and selective

816   attention share similar functional networks, at least in part. Such results also justify labels such

817   as the "successful attention network" (Rosenberg et al., 2018). Importantly, these network

818   overlaps are consistent with both the CPM predictions and the behavioral relationships (Figure

819   4). Significant network overlaps involving the VAB network, however, were not accompanied

820   by significant behavioral relationships. We return to this observation in the Discussion.

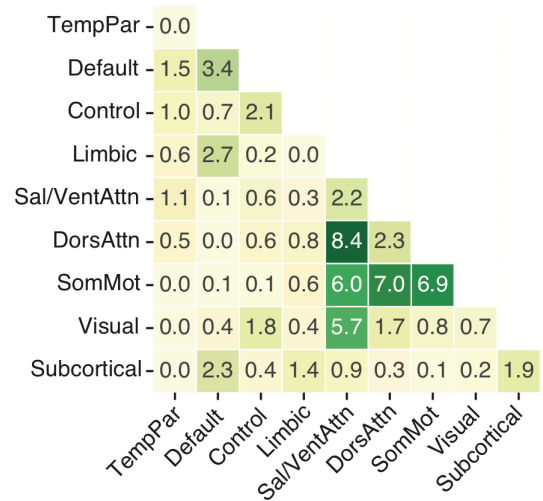821   **Anatomical locations of network edges**

822   To better understand the networks that contribute to the successful behavioral predictions

823 from the vabCPM and the saCPM, we investigated the anatomy of their underlying network

824 edges. Briefly, for each pair of network groups (e.g. Visual and Salience / Ventral Attention), we

825 expressed the number of shared connections (network edges) as a percentage of the number of

826 possible connections between that pair (Figure 9). Edges that positively predicted VAB

827 performance occurred primarily between the Default network and several other networks,

828 including the Salience/Ventral attention, Dorsal attention, and Somatomotor networks (Figure

829 9a). For negative network edges, the most frequent connections occurred between the

830 Salience/Ventral attention network and several other networks, including the Dorsal attention,

831 Somatomotor, and Visual networks (Figure 9b). Note that such connections were also enhanced

832 in VABFC compared to RSFC (Figure 5c), and that the connections across attention networks

833 are consistent with the neural correlates of the attentional blink (Marois et al., 2000; Marois &

834 Ivanoff, 2005). Negative network edges were also frequently found in Somatomotor network

835 connections to the Dorsal attention network and to itself (within-network connections).

836   The SA network's positive edges primarily included connections that involved the Visual

837 and Subcortical network groups (Figure 9d). This pattern represents the remapping of the

838 connections between the cerebellum and the occipital lobe of the "high attention" network

839 (Rosenberg, Finn, et al., 2016) from the Shen-268 parcellation (Shen et al., 2013) to the

840 Schaefer-419 one (Schaefer et al., 2017). Negative network edges included within-group

841 connections in the TempPar and Subcortical networks (Figure 9c), which accord well with the

842 intra-temporal, intra-cerebellar, and temporo-parietal connections in the "low attention" network

843 (Rosenberg, Finn, et al., 2016). We observed additional negative edges within the Visual

844 network and from the TempPar network to various other networks.
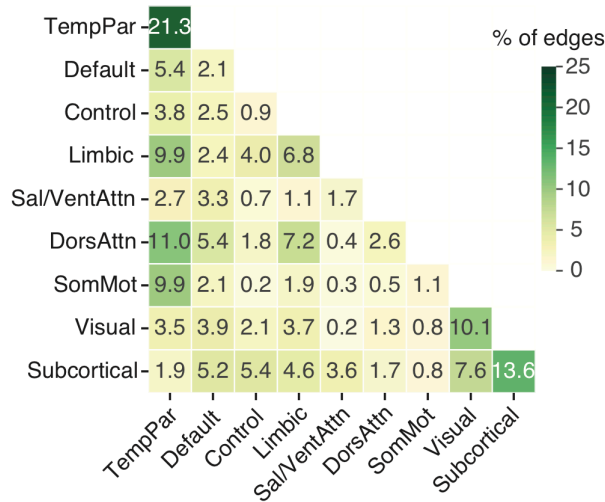
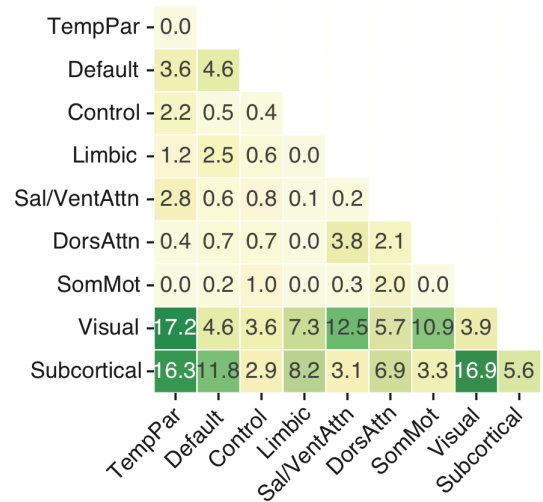(a) VAB, positive network edge locations
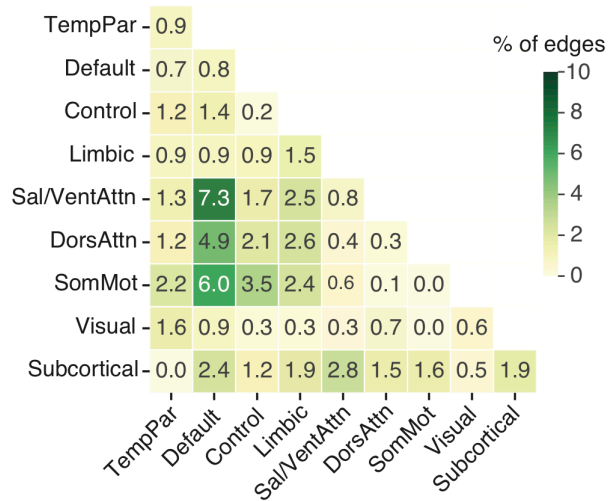
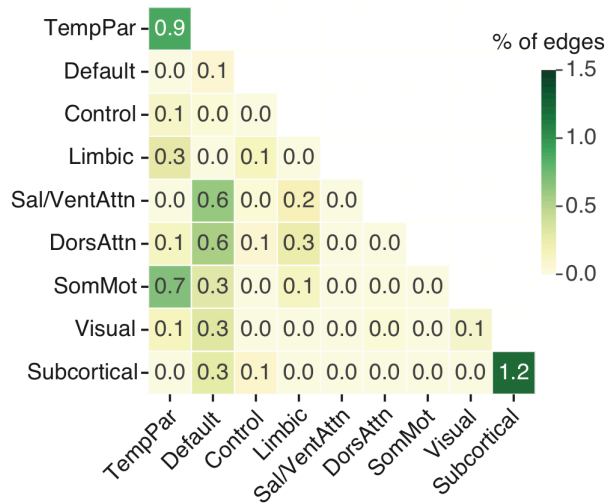(b) VAB, negative network edge locations

(c) SA, negative network edge locations

(d) SA, positive network edge locations

(e) Edge overlap; positive VAB, negative SA

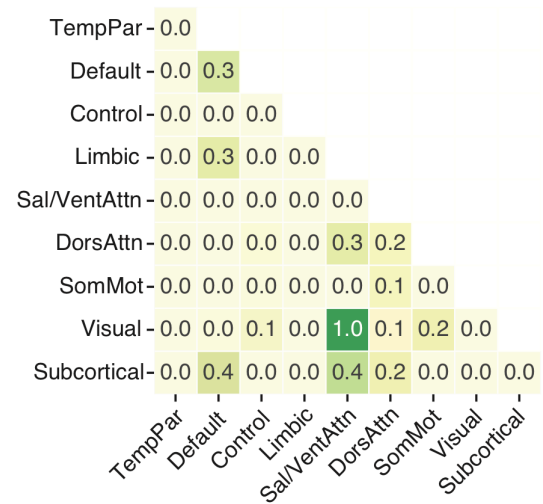(f) Edge overlap; negative VAB, positive SA

845

846   Figure 9. Anatomical locations of predictive attentional network edges. Each cell represents the

847   number of shared connections between a pair of network groups, expressed as a percentage of

848   the number of possible connections between that pair. For details about network groups, see

849   Figure 5. (a) Positive and (b) negative VAB network edges. (c) Negative and (d) positive SA

850   network edges. The panel order has been reversed for easier comparison with the opposing edges

851   from the VAB network. (e) Positive VAB network edges and negative SA network edges (i.e.

852   overlaps between (a) and (c)). (f) Negative VAB network edges and positive SA network edges

853   (i.e. overlaps between (b) and (d)). Overlap percentages were numerically small, but included

854   key network groups, particularly Default and Salience / Ventral Attention (Sal/VentAttn).

855

856   Although the VAB and SA networks involved largely dissociable sets of edges, some

857   critical edges appeared to be shared (Figure 9e and 9f). Note that these overlaps were at opposing

858   edges (Figure 8). Although overlap percentages were numerically small, they included key

859   network groups. In particular, multiple identified connections involved the Default,

860   Salience/Ventral attention, or TempPar networks.

861

862   **Discussion**

863   **Predictive attentional networks**

864   We used Connectome-based Predictive Modeling (CPM), a machine learning-based

865   technique that associates task performance with functional connectivity measures, to construct a

866   predictive model of Visual Attentional Blink (VAB) performance. Our model (vabCPM)

867   successfully predicted VAB performance in novel individuals from fMRI data. The model's

868   predictions generalized to other task domains, including fluid intelligence (Finn et al., 2015).

869   Critically, vabCPM predictions for many sustained and selective attention task scores correlated

870   *negatively* with the actual scores. As such, these significant predictions represent both model

871   generalization and an extension of previous CPM results (Rosenberg, Finn, et al., 2016;

872   Rosenberg et al., 2018; Yoo et al., 2017), but with new insights into attentional function owing to

873   the divergent predictions.

874   For external validation of these results, we applied the Sustained Attention CPM

875   (saCPM) (Rosenberg, Finn, et al., 2016), to our data. Previously, the saCPM successfully

876   predicted task performance for sustained attention (GradCPT) (Rosenberg, Finn, et al., 2016) and

877   selective attention (Attention Network Task, ANT) (Rosenberg et al., 2018). Here we broadly

878   replicated these results: The saCPM successfully predicted sustained and selective attention task

879   performance when applied to our participants' data. In the sustained attention domain, however,

880   significant predictions were found only for visual and auditory SART (Sustained Attention to

881   Response Task) scores, but curiously not for GradCPT scores. In results that mirrored the

882   vabCPM predictions, the saCPM predictions for VAB scores were negatively correlated with the

883   observed scores.

884   This pattern of divergent predictions was also reflected in network overlaps. For the

885   networks derived from the vabCPM and the saCPM, *opposing* network edges (i.e. positive from

886   one, negative from the other) overlapped significantly, whereas similar network edges did not.

887   Models constructed from each behavioral task and our fMRI data corroborated these results. As

888   all behavioral data had been coded such that larger values indicated better performance, these

889   divergent predictions indicate that "good" or "bad" network function was contingent on the task

890   and its cognitive underpinnings. Moreover, the tasks were performed over several days,

47

891   suggesting that the individual differences were stable and trait-like, not due to session-specific

892   state effects.

893   **Implications for Cognitive Mechanisms**

894   Although the observed pattern of CPM predictions may seem counterintuitive, it is

895   consistent with both empirical evidence and theoretical positions. Foremost, our study's attention

896   tasks represent different ways of deploying voluntary attention. The VAB task requires rapid

897   attentional engagement, disengagement, and re-engagement; sustained attention tasks require

898   engagement over a prolonged period of time; the attention network task (ANT) requires the

899   direction of attention to relevant spatial information. Skogsberg et al. (2015) proposed that the

900   VAB and sustained attention tasks lie at opposite ends of a transient-sustained attention

901   continuum. Rensink suggested that the VAB and ANT involve different core attentional

902   functions: In the VAB, 'attentional holding' of one visual object leads to the failure to create a

903   second visual object, whereas in the ANT, 'attentional filtering' selects spatial information

904   (Rensink, 2013, 2015).

905   Empirical findings support the relative uniqueness of the VAB, while also suggesting that

906   the ANT and sustained attention are more closely related. In our data, we found a general lack of

907   behavioral correlations between the VAB and other attention task measures, consistent with

908   previous studies of individual differences (Dale et al., 2013; Skogsberg et al., 2015). Conversely,

909   we found moderately strong correlations between sustained attention tasks and the ANT. These

910   tasks have been found to share similar functional networks (Rosenberg et al., 2018), a result we

911   also replicated.

912   Nevertheless, the conceptual separation of the VAB from other attention tasks does not

913   explain the *opposing* pattern of predictions from the same networks (saCPM and vabCPM), and

914   the significant overlaps between their opposing network edges. Two observations provide

915   important context for this finding. First, the VAB has spawned a variety of theoretical accounts

916   (Dux & Marois, 2009), and its magnitude is sensitive to numerous disparate manipulations,

917   ranging from requiring online responses (Jolicoeur, 1998) to concurrently listening to music

918   (Olivers & Nieuwenhuis, 2005). As such, the VAB may have multiple causes. Second, our VAB

919   predictions were generally moderate (r = .31 for vabCPM and r = .24 for saCPM; 5-10% of the

920   variance), far smaller than the observed degree of stable individual differences (test-retest: r =

921   .71; 50% of the variance). It is possible that the CPMs capture the variance associated with few,

922   or even one, of the factors that affect VAB magnitude. If so, what could that factor be?

923   One plausible explanation is that our predictions reflect an individual's propensity to

924   maintain a more diffuse state of attention. This idea is consistent with the overinvestment

925   hypothesis, in which the VAB results from too much attention being allocated to the first target;

926   consequently, reducing attention on the RSVP stream improves performance (Dale & Arnell,

927   2010, 2015; Olivers & Nieuwenhuis, 2006). Similarly, task-concurrent mind-wandering, such as

928   listening to music or thinking about a vacation, reduces the VAB deficit (Olivers &

929   Nieuwenhuis, 2005, 2006). Similar effects are found in studies of disposition: Individuals with a

930   greater propensity for mind-wandering tend to perform better in the VAB task (Thomson et al.,

931   2015). Furthermore, mind-wandering has been linked to higher fluid intelligence and better

932   problem-solving abilities (Baird, Smallwood, & Schooler, 2011; Godwin et al., 2017; Unsworth

933   & McMillan, 2014), consistent with our CPM findings.

934   Diffuse attentional states, however, are associated with lower performance on tasks

935   requiring more focused cognition. For example, in sustained attention tasks, individuals more

936   prone to lapses in attention perform more poorly on the SART (Manly, 1999; Robertson et al.,

937   1997; Smilek et al., 2010). Within individuals, distractive thoughts are associated with lower

938   SART accuracy, prolonged and more variable RTs, and poorer response inhibition (Kam &

939   Handy, 2014; Leszczynski et al., 2017; Stawarczyk, Majerus, Maj, Van der Linden, &

940   D'Argembeau, 2011). In selective attention tasks, individuals more prone to mind-wandering

941   performed worse on the ANT task (Gonçalves et al., 2017), and showed impaired exogeneous

942   orienting of attention (Hu et al., 2012).

943   Both mind-wandering states and traits are also reflected in patterns of brain activity.

944   Activity in the Default network and frontoparietal control regions increases during mind-

945   wandering (Fox, Spreng, Ellamil, Andrews-Hanna, & Christoff, 2015). Similarly, individuals

946   more prone to mind-wander had increased connectivity both within the Default network and

947   between the Default network and frontoparietal control regions (Godwin et al., 2017). Such

948   results are partially consistent with our findings. Edges between the Default and attentional

949   networks (not the Control network) were related to positive VAB network edges and negative

950   SA network edges.

951   On the weight of the available evidence, we propose that our vabCPM reflects

952   individuals' propensity towards diffuse attentional deployment. That propensity could indicate

953   an individual's ability to diffusely attend, their tendency to be in that state or mode, or both. We

954   also suggest that other CPMs, including the saCPM, could reflect the complementary propensity

955   towards more focused attentional deployment.

956   **Predictions from "Resting State"**

957   Neuroimaging studies using 'resting state' data, in which subjects are scanned while not

958   engaged in any particular task, have become increasingly popular. Initially used to identify

959   functional architecture (Biswal, Yetkin, Haughton, & Hyde, 1995; Schaefer et al., 2017; Yeo et

50

960   al., 2011), resting state data have recently been used to test whether functional architecture

961   persists even when an individual is not engaged in a task that requires a given neurocognitive

962   network (Finn et al., 2015; Jangraw et al., 2018; Lin et al., 2018; Rosenberg, Finn, et al., 2016;

963   Yoo et al., 2017). Resting state studies also have many logistical advantages, including relatively

964   easy standardization across multiple test sites and the potential for numerous applications from a

965   single data set. In the current study, resting state CPMs (Model type D) replicated previous

966   studies by successfully predicting sustained attention (Yoo et al., 2017), selective attention (Yoo

967   et al., 2017) and fluid intelligence (Finn et al., 2015) task performance. We also replicated the

968   result that models trained with *task-concurrent* FC data generally predict task performance better

969   than models trained from resting state data (Yoo et al., 2017). Finally, when applying our trained

970   vabCPM model to novel participants, predictions from task FC data were superior to predictions

971   from resting-state FC data (Finn et al., 2017; Greene, Gao, Scheinost, & Constable, 2018;

972   Rosenberg, Finn, et al., 2016; Rosenberg et al., 2018). This result might be due to amplification

973   of behaviorally relevant individual differences in network patterns while performing a task

974   (Greene et al., 2018).

975   **Methodological Considerations**

976   Although we followed the guidelines in Shen et al. (2017) when developing our CPMs,

977   there are two notable methodological differences. First, previous studies used the volumetric

978   Shen-268 parcellation (Shen et al., 2013), but we used the surface-based Schaefer-419

979   parcellation (Schaefer et al., 2017). Second, previous studies have constructed linear models for

980   associating network strength and behavioral scores, with predictions assessed using Spearman

981   correlations (Fountain-Zaragoza et al., 2019; Lin et al., 2018; Rosenberg, Finn, et al., 2016;

982   Rosenberg et al., 2018). We instead formed linear models from the ranks directly. Despite these

51

983   differences, we still observed prediction patterns that were largely consistent and comparable to

984   previous studies, providing evidence that CPMs are reasonably robust across such variations.

985

986   **References**

987   Adolfsdottir, S., Sorensen, L., & Lundervold, A. J. (2008). The attention network test: A

988   characteristic pattern of deficits in children with ADHD. *Behavioral and Brain*

989   *Functions*, *4*(1), 9. https://doi.org/10.1186/1744-9081-4-9

990   Asplund, C. L., Todd, J. J., Snyder, A. P., & Marois, R. (2010). A central role for the lateral

991   prefrontal cortex in goal-directed and stimulus-driven attention. *Nature Neuroscience*,

992   *13*(4), 507–512. https://doi.org/10.1038/nn.2509

993   Baird, B., Smallwood, J., & Schooler, J. W. (2011). Back to the future: Autobiographical

994   planning and the functionality of mind-wandering. *Consciousness and Cognition*, *20*(4),

995   1604–1611. https://doi.org/10.1016/j.concog.2011.08.007

996   Benjamini, Y., & Hochberg, Y. (1995). Controlling the False Discovery Rate: A Practical and

997   Powerful Approach to Multiple Testing. *Journal of the Royal Statistical Society. Series B*

998   *(Methodological)*, *57*(1), 289–300.

999   Bilker, W. B., Hansen, J. A., Brensinger, C. M., Richard, J., Gur, R. E., & Gur, R. C. (2012).

1000   Development of Abbreviated Nine-Item Forms of the Raven's Standard Progressive

1001   Matrices Test. *Assessment*, *19*(3), 354–369. https://doi.org/10.1177/1073191112446655

1002   Biswal, B., Yetkin, F. Z., Haughton, V. M., & Hyde, J. S. (1995). Functional connectivity in the

1003   motor cortex of resting human brain using echo-planar MRI. *Magnetic Resonance in*

1004   *Medicine*, *34*(4), 537–541.

1005   Chun, M. M., Golomb, J. D., & Turk-Browne, N. B. (2011). A Taxonomy of External and

1006   Internal Attention. *Annual Review of Psychology*, *62*(1), 73–101.

1007   https://doi.org/10.1146/annurev.psych.093008.100427

1008   Chun, M. M., & Potter, M. C. (1995). A two-stage model for multiple target detection in rapid

1009   serial visual presentation. *Journal of Experimental Psychology. Human Perception and*

1010   *Performance*, *21*(1), 109–127.

1011   Corbetta, M., & Shulman, G. L. (2002). Control of goal-directed and stimulus-driven attention in

1012   the brain. *Nature Reviews Neuroscience*, *3*(3), 201–215. https://doi.org/10.1038/nrn755

1013   Dale, G., & Arnell, K. M. (2010). Individual differences in dispositional focus of attention

1014   predict attentional blink magnitude. *Attention, Perception, & Psychophysics*, *72*(3), 602–

1015   606. https://doi.org/10.3758/APP.72.3.602

1016   Dale, G., & Arnell, K. M. (2015). Multiple measures of dispositional global/local bias predict

1017   attentional blink magnitude. *Psychological Research*, *79*(4), 534–547.

1018   https://doi.org/10.1007/s00426-014-0591-3

1019   Dale, G., Dux, P. E., & Arnell, K. M. (2013). Individual differences within and across attentional

1020   blink tasks revisited. *Attention, Perception, & Psychophysics*, *75*(3), 456–467.

1021   https://doi.org/10.3758/s13414-012-0415-8

1022   Desimone, R., & Duncan, J. (1995). Neural Mechanisms of Selective Visual Attention. *Annual*

1023   *Review of Neuroscience*, *18*(1), 193–222.

1024   https://doi.org/10.1146/annurev.ne.18.030195.001205

1025   Di Lollo, V., Kawahara, J., Shahab Ghorashi, S. M., & Enns, J. T. (2005). The attentional blink:

1026   Resource depletion or temporary loss of control? *Psychological Research*, *69*(3), 191–

1027   200. https://doi.org/10.1007/s00426-004-0173-x

1028   Duncan, J. (2010). The multiple-demand (MD) system of the primate brain: Mental programs for

1029   intelligent behaviour. *Trends in Cognitive Sciences*, *14*(4), 172–179.

1030   https://doi.org/10.1016/j.tics.2010.01.004

1031   Dux, P. E., & Marois, R. (2009). The attentional blink: A review of data and theory. *Attention,*

1032   *Perception & Psychophysics*, *71*(8), 1683–1700. https://doi.org/10.3758/APP.71.8.1683

1033   Egeth, H. E., & Yantis, S. (1997). Visual attention: Control, representation, and time course.

1034   *Annual Review of Psychology*, *48*(1), 269–297.

1035   Esterman, M., Noonan, S. K., Rosenberg, M., & DeGutis, J. (2013). In the Zone or Zoning Out?

1036   Tracking Behavioral and Neural Fluctuations During Sustained Attention. *Cerebral*

1037   *Cortex*, *23*(11), 2712–2723. https://doi.org/10.1093/cercor/bhs261

1038   Fan, J., McCandliss, B. D., Sommer, T., Raz, A., & Posner, M. I. (2002). Testing the Efficiency

1039   and Independence of Attentional Networks. *Journal of Cognitive Neuroscience*, *14*(3),

1040   340–347. https://doi.org/10.1162/089892902317361886

1041   Feinberg, D. A., Moeller, S., Smith, S. M., Auerbach, E., Ramanna, S., Glasser, M. F., …

1042   Yacoub, E. (2010). Multiplexed Echo Planar Imaging for Sub-Second Whole Brain

1043   FMRI and Fast Diffusion Imaging. *PLoS ONE*, *5*(12), e15710.

1044   https://doi.org/10.1371/journal.pone.0015710

1045   Finn, E. S., Scheinost, D., Finn, D. M., Shen, X., Papademetris, X., & Constable, R. T. (2017).

1046   Can brain state be manipulated to emphasize individual differences in functional

1047   connectivity? *NeuroImage*, *160*, 140–151.

1048   https://doi.org/10.1016/j.neuroimage.2017.03.064

1049   Finn, E. S., Shen, X., Scheinost, D., Rosenberg, M. D., Huang, J., Chun, M. M., … Constable, R.

1050   T. (2015). Functional connectome fingerprinting: Identifying individuals using patterns

1051   of brain connectivity. *Nature Neuroscience*, *18*(11), 1664–1671.

1052   https://doi.org/10.1038/nn.4135

1053   Fong, A. H. C., Yoo, K., Rosenberg, M. D., Zhang, S., Li, C.-S. R., Scheinost, D., … Chun, M.

1054   M. (2019). Dynamic functional connectivity during task performance and rest predicts

1055   individual differences in attention across studies. *NeuroImage*, *188*, 14–25.

1056   https://doi.org/10.1016/j.neuroimage.2018.11.057

1057   Fountain-Zaragoza, S., Samimy, S., Rosenberg, M. D., & Prakash, R. S. (2019). Connectome-

1058   based models predict attentional control in aging adults. *NeuroImage*, *186*, 1–13.

1059   https://doi.org/10.1016/j.neuroimage.2018.10.074

1060   Fox, K. C. R., Spreng, R. N., Ellamil, M., Andrews-Hanna, J. R., & Christoff, K. (2015). The

1061   wandering brain: Meta-analysis of functional neuroimaging studies of mind-wandering

1062   and related spontaneous thought processes. *NeuroImage*, *111*, 611–621.

1063   https://doi.org/10.1016/j.neuroimage.2015.02.039

1064   Godwin, C. A., Hunter, M. A., Bezdek, M. A., Lieberman, G., Elkin-Frankston, S., Romero, V.

1065   L., … Schumacher, E. H. (2017). Functional connectivity within and between intrinsic

1066   brain networks correlates with trait mind wandering. *Neuropsychologia*, *103*, 140–153.

1067   https://doi.org/10.1016/j.neuropsychologia.2017.07.006

1068   Gonçalves, Ó. F., Rêgo, G., Oliveira-Silva, P., Leite, J., Carvalho, S., Fregni, F., … Boggio, P. S.

1069   (2017). Mind wandering and the attention network system. *Acta Psychologica*, *172*, 49–

1070   54. https://doi.org/10.1016/j.actpsy.2016.11.008

1071   Greene, A. S., Gao, S., Scheinost, D., & Constable, R. T. (2018). Task-induced brain state

1072   manipulation improves prediction of individual traits. *Nature Communications*, *9*(1).

1073   https://doi.org/10.1038/s41467-018-04920-3

1074   Hu, N., He, S., & Xu, B. (2012). Different efficiencies of attentional orienting in different

1075   wandering minds. *Consciousness and Cognition*, *21*(1), 139–148.

1076   https://doi.org/10.1016/j.concog.2011.12.007

1077   Jangraw, D. C., Gonzalez-Castillo, J., Handwerker, D. A., Ghane, M., Rosenberg, M. D.,

1078   Panwar, P., & Bandettini, P. A. (2018). A functional connectivity-based neuromarker of

1079   sustained attention generalizes to predict recall in a reading task. *NeuroImage*, *166*, 99–

1080   109. https://doi.org/10.1016/j.neuroimage.2017.10.019

1081   Jolicoeur, P. (1998). Modulation of the attentional blink by on-line response selection: Evidence

1082   from speeded and unspeeded Task1 decisions. *Memory & Cognition*, *26*(5), 1014–1032.

1083   https://doi.org/10.3758/BF03201180

1084   Kam, J. W. Y., & Handy, T. C. (2014). Differential recruitment of executive resources during

1085   mind wandering. *Consciousness and Cognition*, *26*, 51–63.

1086   https://doi.org/10.1016/j.concog.2014.03.002

1087   Kong, R., Li, J., Orban, C., Sabuncu, M. R., Liu, H., Schaefer, A., … Yeo, B. T. T. (2019).

1088   Spatial Topography of Individual-Specific Cortical Networks Predicts Human Cognition,

1089   Personality, and Emotion. *Cerebral Cortex*, *29*(6), 2533–2551.

1090   https://doi.org/10.1093/cercor/bhy123

1091   Leszczynski, M., Chaieb, L., Reber, T. P., Derner, M., Axmacher, N., & Fell, J. (2017). Mind

1092   wandering simultaneously prolongs reactions and promotes creative incubation. *Scientific*

1093   *Reports*, *7*(1). https://doi.org/10.1038/s41598-017-10616-3

1094   Lin, Q., Rosenberg, M. D., Yoo, K., Hsu, T. W., O'Connell, T. P., & Chun, M. M. (2018).

1095   Resting-State Functional Connectivity Predicts Cognitive Impairment Related to

1096   Alzheimer's Disease. *Frontiers in Aging Neuroscience*, *10*.

1097   https://doi.org/10.3389/fnagi.2018.00094

1098   Lundervold, A. J., Adolfsdottir, S., Halleland, H., Halmøy, A., Plessen, K., & Haavik, J. (2011).

1099   Attention Network Test in adults with ADHD - the impact of affective fluctuations.

1100   *Behavioral and Brain Functions*, *7*(1), 27. https://doi.org/10.1186/1744-9081-7-27

1101   MacLean, M. H., & Arnell, K. M. (2012). A conceptual and methodological framework for

1102   measuring and modulating the attentional blink. *Attention, Perception, & Psychophysics*,

1103   *74*(6), 1080–1097. https://doi.org/10.3758/s13414-012-0338-4

1104   Manly, T. (1999). The absent mind: Further investigations of sustained attention to response.

1105   *Neuropsychologia*, *37*(6), 661–670. https://doi.org/10.1016/S0028-3932(98)00127-4

1106   Marois, R., Chun, M. M., & Gore, J. C. (2000). Neural correlates of the attentional blink.

1107   *Neuron*, *28*(1), 299–308.

1108   Marois, R., & Ivanoff, J. (2005). Capacity limits of information processing in the brain. *Trends*

1109   *in Cognitive Sciences*, *9*(6), 296–305. https://doi.org/10.1016/j.tics.2005.04.010

1110   *MATLAB*. (2014). Natick, MA: The MathWorks, Inc.

1111   Moeller, S., Yacoub, E., Olman, C. A., Auerbach, E., Strupp, J., Harel, N., & Uğurbil, K. (2010).

1112   Multiband multislice GE-EPI at 7 tesla, with 16-fold acceleration using partial parallel

1113   imaging with application to high spatial and temporal whole-brain fMRI. *Magnetic*

1114   *Resonance in Medicine*, *63*(5), 1144–1153. https://doi.org/10.1002/mrm.22361

1115   Olivers, C. N. L., & Nieuwenhuis, S. (2005). The Beneficial Effect of Concurrent Task-

1116   Irrelevant Mental Activity on Temporal Attention. *Psychological Science*, *16*(4), 265–

1117   269. https://doi.org/10.1111/j.0956-7976.2005.01526.x

1118 Olivers, C. N. L., & Nieuwenhuis, S. (2006). The beneficial effects of additional task load,

1119 positive affect, and instruction on the attentional blink. *Journal of Experimental*

1120 *Psychology: Human Perception and Performance*, *32*(2), 364–379.

1121 https://doi.org/10.1037/0096-1523.32.2.364

1122 Peirce, J. W. (2007). PsychoPy—Psychophysics software in Python. *Journal of Neuroscience*

1123 *Methods*, *162*(1–2), 8–13. https://doi.org/10.1016/j.jneumeth.2006.11.017

1124 Posner, M. I., & Petersen, S. E. (1990). The Attention System of the Human Brain. *Annual*

1125 *Review of Neuroscience*, *13*(1), 25–42.

1126 https://doi.org/10.1146/annurev.ne.13.030190.000325

1127 Power, J. D., Barnes, K. A., Snyder, A. Z., Schlaggar, B. L., & Petersen, S. E. (2012). Spurious

1128 but systematic correlations in functional connectivity MRI networks arise from subject

1129 motion. *NeuroImage*, *59*(3), 2142–2154.

1130 https://doi.org/10.1016/j.neuroimage.2011.10.018

1131 Power, J. D., Mitra, A., Laumann, T. O., Snyder, A. Z., Schlaggar, B. L., & Petersen, S. E.

1132 (2014). Methods to detect, characterize, and remove motion artifact in resting state fMRI.

1133 *NeuroImage*, *84*, 320–341. https://doi.org/10.1016/j.neuroimage.2013.08.048

1134 Raven, J., Raven, J. C., & Court, J. H. (1998). *Manual for Raven's progressive matrices and*

1135 *vocabulary scales*. Oxford: Oxford Psychologists.

1136 Raymond, J. E., Shapiro, K. L., & Arnell, K. M. (1992). Temporary suppression of visual

1137 processing in an RSVP task: An attentional blink? *Journal of Experimental Psychology.*

1138 *Human Perception and Performance*, *18*(3), 849–860.

1139 Rensink, R. A. (2013). Perception and Attention. In D. Reisberg (Ed.), *Oxford Handbook of*

1140 *Cognitive Psychology* (pp. 97–116). New York: Oxford University Press.

1141 Rensink, R. A. (2015). A Function-Centered Taxonomy of Visual Attention. In P. Coates & S.

1142 Coleman (Eds.), *Phenomenal Qualities: Sense, Perception, and Consciousness*. (pp. 347–

1143 375). Oxford: Oxford University Press.

1144 Robertson, I. H., Manly, T., Andrade, J., Baddeley, B. T., & Yiend, J. (1997). `Oops!':

1145 Performance correlates of everyday attentional failures in traumatic brain injured and

1146 normal subjects. *Neuropsychologia*, *35*(6), 747–758. https://doi.org/10.1016/S0028-

1147 3932(97)00015-8

1148 Rosenberg, M. D., Finn, E. S., Scheinost, D., Papademetris, X., Shen, X., Constable, R. T., &

1149 Chun, M. M. (2016). A neuromarker of sustained attention from whole-brain functional

1150 connectivity. *Nature Neuroscience*, *19*(1), 165–171. https://doi.org/10.1038/nn.4179

1151 Rosenberg, M. D., Hsu, W.-T., Scheinost, D., Constable, T. R., & Chun, M. M. (2018).

1152 Connectome-based Models Predict Separable Components of Attention in Novel

1153 Individuals. *Journal of Cognitive Neuroscience*, *30*(2), 160–173.

1154 https://doi.org/10.1162/jocn_a_01197

1155 Rosenberg, M. D., Noonan, S., DeGutis, J., & Esterman, M. (2013). Sustaining visual attention

1156 in the face of distraction: A novel gradual-onset continuous performance task. *Attention,*

1157 *Perception, & Psychophysics*, *75*(3), 426–439. https://doi.org/10.3758/s13414-012-0413-

1158 x

1159 Rosenberg, M. D., Zhang, S., Hsu, W.-T., Scheinost, D., Finn, E. S., Shen, X., … Chun, M. M.

1160 (2016). Methylphenidate Modulates Functional Network Connectivity to Enhance

1161 Attention. *Journal of Neuroscience*, *36*(37), 9547–9557.

1162 https://doi.org/10.1523/JNEUROSCI.1746-16.2016

Schaefer, A., Kong, R., Gordon, E. M., Laumann, T. O., Zuo, X.-N., Holmes, A. J., … Yeo, B. T. T. (2017). Local-Global Parcellation of the Human Cerebral Cortex from Intrinsic Functional Connectivity MRI. *Cerebral Cortex*, 1–20. https://doi.org/10.1093/cercor/bhx179

Seli, P., Cheyne, J. A., Barton, K. R., & Smilek, D. (2012). Consistency of sustained attention across modalities: Comparing visual and auditory versions of the SART. *Canadian Journal of Experimental Psychology/Revue Canadienne de Psychologie Expérimentale*, *66*(1), 44–50. https://doi.org/10.1037/a0025111

Shen, X., Finn, E. S., Scheinost, D., Rosenberg, M. D., Chun, M. M., Papademetris, X., & Constable, R. T. (2017). Using connectome-based predictive modeling to predict individual behavior from brain connectivity. *Nature Protocols*, *12*(3), 506–518. https://doi.org/10.1038/nprot.2016.178

Shen, X., Tokoglu, F., Papademetris, X., & Constable, R. T. (2013). Groupwise whole-brain parcellation from resting-state fMRI data for network node identification. *NeuroImage*, *82*, 403–415. https://doi.org/10.1016/j.neuroimage.2013.05.081

Skogsberg, K., Grabowecky, M., Wilt, J., Revelle, W., Iordanescu, L., & Suzuki, S. (2015). A relational structure of voluntary visual-attention abilities. *Journal of Experimental Psychology: Human Perception and Performance*, *41*(3), 761–789. https://doi.org/10.1037/a0039000

Smilek, D., Carriere, J. S. A., & Cheyne, J. A. (2010). Failures of sustained attention in life, lab, and brain: Ecological validity of the SART. *Neuropsychologia*, *48*(9), 2564–2570. https://doi.org/10.1016/j.neuropsychologia.2010.05.002

1185   Stawarczyk, D., Majerus, S., Maj, M., Van der Linden, M., & D'Argembeau, A. (2011). Mind-

1186   wandering: Phenomenology and function as assessed with a novel experience sampling

1187   method. *Acta Psychologica*, *136*(3), 370–381.

1188   https://doi.org/10.1016/j.actpsy.2011.01.002

1189   Tamber-Rosenau, B. J., Dux, P. E., Tombu, M. N., Asplund, C. L., & Marois, R. (2013). Amodal

1190   Processing in Human Prefrontal Cortex. *Journal of Neuroscience*, *33*(28), 11573–11587.

1191   https://doi.org/10.1523/JNEUROSCI.4601-12.2013

1192   Thomson, D. R., Ralph, B. C. W., Besner, D., & Smilek, D. (2015). The more your mind

1193   wanders, the smaller your attentional blink: An individual differences study. *Quarterly*

1194   *Journal of Experimental Psychology*, *68*(1), 181–191.

1195   https://doi.org/10.1080/17470218.2014.940985

1196   Unsworth, N., & McMillan, B. D. (2014). Similarities and differences between mind-wandering

1197   and external distraction: A latent variable analysis of lapses of attention and their relation

1198   to cognitive abilities. *Acta Psychologica*, *150*, 14–25.

1199   https://doi.org/10.1016/j.actpsy.2014.04.001

1200   Van Dijk, K. R. A., Hedden, T., Venkataraman, A., Evans, K. C., Lazar, S. W., & Buckner, R. L.

1201   (2010). Intrinsic functional connectivity as a tool for human connectomics: Theory,

1202   properties, and optimization. *Journal of Neurophysiology*, *103*(1), 297–321.

1203   https://doi.org/10.1152/jn.00783.2009

1204   Webb, G. I., Sammut, C., Perlich, C., Horváth, T., Wrobel, S., Korb, K. B., … Raedt, L. D.

1205   (2011). Leave-One-Out Cross-Validation. In C. Sammut & G. I. Webb (Eds.),

1206   *Encyclopedia of Machine Learning* (pp. 600–601). https://doi.org/10.1007/978-0-387-

1207   30164-8_469

1208   Wojtowicz, M., Berrigan, L. I., & Fisk, J. D. (2012). Intra-individual Variability as a Measure of

1209   Information Processing Difficulties in Multiple Sclerosis. *International Journal of MS*

1210   *Care*, *14*(2), 77–83. https://doi.org/10.7224/1537-2073-14.2.77

1211   Xu, J., Moeller, S., Auerbach, E. J., Strupp, J., Smith, S. M., Feinberg, D. A., … Uğurbil, K.

1212   (2013). Evaluation of slice accelerations using multiband echo planar imaging at 3T.

1213   *NeuroImage*, *83*, 991–1001. https://doi.org/10.1016/j.neuroimage.2013.07.055

1214   Yeo, B. T. T., Krienen, F. M., Eickhoff, S. B., Yaakub, S. N., Fox, P. T., Buckner, R. L., …

1215   Chee, M. W. L. (2015). Functional Specialization and Flexibility in Human Association

1216   Cortex. *Cerebral Cortex*, *25*(10), 3654–3672. https://doi.org/10.1093/cercor/bhu217

1217   Yeo, B. T. T., Krienen, F. M., Sepulcre, J., Sabuncu, M. R., Lashkari, D., Hollinshead, M., …

1218   Buckner, R. L. (2011). The organization of the human cerebral cortex estimated by

1219   intrinsic functional connectivity. *Journal of Neurophysiology*, *106*(3), 1125–1165.

1220   https://doi.org/10.1152/jn.00338.2011

1221   Yeo, B. T. T., Tandi, J., & Chee, M. W. L. (2015). Functional connectivity during rested

1222   wakefulness predicts vulnerability to sleep deprivation. *NeuroImage*, *111*, 147–158.

1223   https://doi.org/10.1016/j.neuroimage.2015.02.018

1224   Yoo, K., Rosenberg, M. D., Hsu, W.-T., Zhang, S., Li, C.-S. R., Scheinost, D., … Chun, M. M.

1225   (2017). Connectome-based predictive modeling of attention: Comparing different

1226   functional connectivity features and prediction methods across datasets. *NeuroImage*.

1227   https://doi.org/10.1016/j.neuroimage.2017.11.010

1228   Zalesky, A., Fornito, A., & Bullmore, E. T. (2010). Network-based statistic: Identifying

1229   differences in brain networks. *NeuroImage*, *53*(4), 1197–1207.

1230   https://doi.org/10.1016/j.neuroimage.2010.06.041

Legends

1231

1232   Table 1. Schedule of tasks and data used in analysis. Participants were encouraged to take breaks

1233   between the tasks to prevent fatigue. With the exception of the Raven's Progressive Matrices

1234   test, each task was performed twice on non-successive days. Task domains and tasks were as

1235   follows. Attentional Blink: Visual Attentional Blink (VAB) and Auditory Attentional Blink

1236   (AAB). Sustained Attention: Visual Sustained Attention to Response Task (VSART), Auditory

1237   Sustained Attention to Response Task (ASART), and Gradual-onset Continuous Performance

1238   Task (GradCPT). Selective Attention: Attentional Network Task (ANT). Fluid Intelligence:

1239   Raven's Progressive Matrices test (Raven's).

1240

1241   Figure 1. Experimental paradigm for the visual attentional blink (VAB) task. Participants

1242   identified a target and then detected a probe within a stream of distractors, responding when

1243   prompted at the conclusion of the stream. The target was a red letter, the probe was a white letter

1244   X, and distractors were other white letters. The auditory attentional blink (AAB) task was

1245   similar, save targets were complex tones, the probe was a high-pitched pure tone, and distractors

1246   were other pure tones. SOA = stimulus onset asynchrony.

1247

1248   Table 2. Summary of behavioral metrics, including their task domain and a description of their

1249   calculation. Raw values for ANTerr, ANTrtvar and ANTcert were re-coded such that larger

1250   values indicated better task performance.

1251

1252   Figure 2. Procedure for Connectome-based Predictive Model (CPM) construction in the current

1253   study (adapted from Shen et al., 2017). CPMs predict individual differences in behavior from

1254   functional connectivity information. (a) Functional connectivity matrices and a behavioral score

1255   of interest for each participant were calculated. One pair was held out of model construction for

1256   each round of leave-one-out cross-validation (LOOCV) (Webb et al., 2011). (b) Functional

1257   connectivity edges were correlated with behavior across participants. (c) Edges that correlated

1258   most strongly, either positively or negatively, were selected. (d) Values from selected edges were

1259   summed separately for positive and negative network edges, yielding two network strengths for

1260   each participant. (e) A linear regression model relating (rank) network strengths to (rank)

1261   behavioral scores was computed. (f) The model was tested on a novel, out-of-sample participant

1262   (the individual left out in step (a)). After repeating steps a-f for each participant, the model was

1263   evaluated by correlating the predicted behavioral scores with the actual scores.

1264

1265   Figure 3. Accuracy scores (probe hit rates) for the VAB and AAB. Note the substantial

1266   impairment for the short target-probe lags (1, 2, and 3) in each session, especially for the VAB.

1267   Error bars represent standard error of the mean (SEM).

1268

1269   Table 3. Summary of behavioral data. Test-retest reliability (Spearman correlations across

1270   sessions) was high for most metrics and significant for all (ps < .002). Jarque-Bera tests indicated

1271   some significant departures from normality. Metrics are presented before re-coding. Metrics that

1272   were subsequently reversed so that larger values would indicate better task performance are

1273   marked with an asterisk (*). N = 73 for all metrics except AABresid (N = 71).

1274

1275   Figure 4. Behavioral score distributions and correlations. (Above diagonal) Spearman correlation

1276   coefficients for pairs of behavioral metrics. Most significant correlations were found within task

1277   domains, but some metrics correlated across the Sustained and Selective Attention domains. In

1278   contrast, Attentional Blink and Fluid Intelligence metrics largely did not correlate with other

1279   metrics. Since the purpose of this analysis was to identify any behavioral relationships that might

1280   explain subsequent CPM results, no correction for multiple comparisons was applied. $*p < .05$,

1281 $**p < .01$. Red and blue shading indicates positive and negative relationships, respectively.

1282   (Diagonal) Histograms of behavioral data. The behavioral data had been re-coded so that larger

1283   values indicate better task performance for each measure. (Below diagonal) Scatterplots for each

1284   pair of behavioral metrics.

1285

1286   Figure 5. Functional connectivity (FC) matrices. Each edge was Fisher-transformed, and the

1287   resulting z-scores were averaged across participants. Edges found to correlate with motion were

1288   set to zero. (a) VAB task FC matrix (VABFC). (b) Resting-state FC matrix (RSFC). VABFC and

1289   RSFC patterns were similar to one another and to other data sets (Yeo et al., 2011; Yeo, Tandi, et

1290   al., 2015). (c) Difference FC matrix (VABFC - RSFC), showing edges that were significant at p

1291 $= .05$, corrected for multiple comparisons using network-based statistics. Differences between

1292   FC matrices were small, though they notably included connections linking the Salience/Ventral

1293   attention and the Dorsal attention networks. The 419 parcellations from the FC matrices were

1294   matched to 17 network labels (Yeo et al., 2011) (green labels), from which they were aggregated

1295   into eight cortical groups (Yeo, Tandi, et al., 2015) and a subcortical group (blue labels, spelled

1296   out in full in (a)). Subcortical regions include the brain stem, accumbens area, amygdala,

1297   caudate, cerebellum, ventral diencephalon, hippocampus, pallidum, putamen, and thalamus. For

1298   the green labels, letters represent the networks within the corresponding group, e.g., a(Default

1299   A), b(Default B), c(Default C), tp(TempPar), t(temporal pole in limbic region), o(orbital frontal

1300   cortex in limbic region), p(peripheral visual area), c(central visual area), and sc(subcortical).

1301

1302   Figure 6. Behavioral predictions from CPMs. Each point represents a pair of Spearman's rank

1303   correlation coefficients (r_s) computed between observed and predicted behavioral scores for a

1304   given model type. (a) Predictions from vabCPMs, which were trained with VABFC and

1305   VABresid. Note the successful positive predictions for the VAB and Fluid Intelligence, but

1306   successful *negative* predictions for some Selective and Sustained Attention metrics. (b)

1307   Predictions from task-specific models. Many models could successfully predict behavioral

1308   performance, though results often varied greatly across the FC source. For both panels, the dark

1309   gray region indicates where r_s values are significant at the $p = .01$ level, and the lighter gray

1310   region indicates where r_s values are significant at the $p = .05$ level (uncorrected, with $d.f. = 71$).

1311   The r_s values and corresponding p-values are tabulated in Figure 6-1 in Extended Data. A

1312   standard edge selection threshold ($r_{threshold} = .232$, $p = .05$) was used for all models, though

1313   results were similar across a wide range of threshold values (Figure 6-2 and Figure 6-3 in

1314   Extended Data). Finally, as p-values from LOOCV procedures can be biased, we verified our

1315   results for the VAB using permutation testing; significance from this method and parametric

1316   approaches was consistent across edge selection thresholds (Figure 6-4 in in Extended Data).

1317

1318   Figure 7. Comparison of predictions from the vabCPM and saCPM. Each point represents a pair

1319   of Spearman's rank correlation coefficients (r_s) computed between observed and predicted

1320   behavioral scores for a given model type. (a) Predictions from VABFC data. Note the saCPM's

1321   successful positive predictions for some Selective and Sustained Attention metrics, with a

1322   successful *negative* prediction for the VAB. As noted above, the prediction directions were

1323   reversed for the vabCPM; indeed, the prediction points fall close to the diagonal. (b) Predictions

1324   from RSFC data. The vabCPM and saCPM predictions went in opposite directions, and were

1325   generally similar to the predictions from the VABFC. For both panels, the dark gray region

1326   indicates where r_s values are significant at the p = .01 level, and the lighter gray region indicates

1327   where r_s values are significant at the p = .05 level (uncorrected, with *d.f.* = 71). The edge

1328   selection threshold ($r_{\text{threshold}}$) corresponded to p = .05 for all models. The r_s values and

1329   corresponding *p*-values for the saCPM are tabulated in Figure 7-1 in the Extended Data. (See

1330   Figure 6 for additional vabCPM details.)

1331

1332   Figure 8. Percentage of edge overlap between networks from selected pairs of CPMs. Each task-

1333   specific model was based on VABFC data (Model type C). Model pairs with statistically

1334   significant overlap (p < .05, FDR corrected) are indicated in bold. Positive network edges

1335   predicted better behavioral performance for their associated metric, whereas negative network

1336   edges predicted worse behavioral performance. Overlap between *similar* network edges, (a)

1337   positive-positive and (b) negative-negative. Sustained Attention (including the saCPM) and

1338   Selective Attention models overlap primarily on similar edges, as do Fluid Intelligence and the

1339   vabCPM. Overlap between *opposing* network edges, (c) negative-positive and (d) positive-

1340   negative. The vabCPM network primarily overlaps with Sustained Attention (including the

1341   saCPM) and Selective Attention on their opposing edges. Only task metrics that were

1342   significantly predicted by vabCPMs using VABFC information are shown. The full set of

1343   overlaps for all CPMs can be found in the Extended Data (Figure 8-1, 8-2, 8-3, and 8-4). Note

68

1344   that the highest overlap value for any pairwise comparison, including each task metric predicted

1345   from VABFC and RSFC, was 26.5%.

1346

1347   Figure 9. Anatomical locations of predictive attentional network edges. Each cell represents the

1348   number of shared connections between a pair of network groups, expressed as a percentage of

1349   the number of possible connections between that pair. For details about network groups, see

1350   Figure 5. (a) Positive and (b) negative VAB network edges. (c) Negative and (d) positive SA

1351   network edges. The panel order has been reversed for easier comparison with the opposing edges

1352   from the VAB network. (e) Positive VAB network edges and negative SA network edges (i.e.

1353   overlaps between (a) and (c)). (f) Negative VAB network edges and positive SA network edges

1354   (i.e. overlaps between (b) and (d)). Overlap percentages were numerically small, but included

1355   key network groups, particularly Default and Salience / Ventral Attention (Sal/VentAttn).

1356

1357   Table 1-1. Detailed protocol from the full study from which the present data derives.

1358

1359   Figure 6-1. Behavioral predictions from CPMs. Values indicate r_s and uncorrected, two-tailed p-

1360   values from Spearman's partial rank correlation, computed between predicted and observed

1361   behavioral scores, controlled for motion. The p-value corresponding to each r_s was found by

1362   transforming the correlation coefficients to Student's t values by the partialcorr.m function in

1363   (*MATLAB*, 2014). Degrees of freedom for these tests were 66 for Models A and C, and 61 for

1364   Models B and D. (For AABresid, these $d.f.$ values were 2 lower.) Note that all task scores had

1365   been re-oriented so that larger values indicate better task performance.

1366

69

1367   Figure 6-2. CPM predictions for models trained with VAB functional connectivity and

1368   behavioral data (Model types A and B) across edge selection thresholds. Within each subplot, the

1369   y-axis represents Spearman's rank correlation values, r_s, computed between predicted and

1370   observed task performance, controlled for motion. Horizontal gray lines indicate the

1371   corresponding p = .01, .05, .10, .10, .05, .01 (top to bottom) uncorrected levels of significance

1372   from standard r-to-p conversions, $d.f.$ = 71 (69 for AAB). The x-axis represents edge selection

1373   thresholds, $r_{threshold}$. The vertical gray line indicates the $r_{threshold}$ at the p = .05 level of

1374   significance, $d.f.$ = 70 (68 for AAB) due to one left-out participant during training. X-axis labels

1375   at the top of each plot indicate the average number of edges selected across all leave-one-out

1376   iterations at the corresponding $r_{threshold}$ on the bottom x-axis.

1377

1378   Figure 6-3. CPM predictions for models trained from task-specific behavioral data (Model types

1379   C and D) across edge selection thresholds. Within each subplot, the y-axis represents Spearman's

1380   rank correlation values, r_s, computed between predicted and observed task performance,

1381   controlled for motion. Horizontal gray lines indicate the corresponding p = .01, .05, .10, .10, .05,

1382   .01 (top to bottom) uncorrected levels of significance from standard r-to-p conversions, $d.f.$ = 71

1383   (69 for AAB). The x-axis represents edge selection thresholds, $r_{threshold}$. The vertical gray line

1384   indicates the $r_{threshold}$ at the p = .05 level of significance, $d.f.$ = 70 (68 for AAB) due to one left-

1385   out participant during training. X-axis labels at the top of each plot indicate the average number

1386   of edges selected across all leave-one-out iterations at the corresponding $r_{threshold}$ on the bottom x-

1387   axis.

1388

1389 Figure 6-4. Permutation results of predicting VABresid data from VAB FC information, using

1390 the vabCPM (Model type A). The black line indicates Spearman's rank correlation values (r_s)

1391 computed between predicted and observed task performance, controlled for motion. Horizontal

1392 gray lines indicate the corresponding p = .01, .05, .10, .10, .05, .01 (top to bottom) uncorrected

1393 levels of significance from standard r-to-p conversions, based on N = 73. Green sections indicate

1394 p < .05 level of significance from permutation testing. Magenta sections indicate $p \geq$. 05 level

1395 of significance from permutation testing. Our analysis demonstrates a high level of consistency

1396 in the significance of r_s values between using standard r-to-p conversions (black line) and using

1397 permutation testing (green/magenta line) for the majority of edge selection thresholds.

1398

1399 Figure 7-1. Results of applying the saCPM model to data in the present study. Values indicate r_s

1400 and uncorrected, two-tailed p-values from Spearman's rank correlation, computed between

1401 predicted and observed behavioral scores. The p-value corresponding to each r_s was found using

1402 standard r-to-p conversions, with $d.f.$ = 71 (69 for AABresid). All task scores had been re-coded

1403 so that larger values indicate better task performance.

1404

1405 Figure 8-1. Percentage of edge overlap for positive network edges between each pair of models.

1406 The value within each cell indicates the percentage of overlap between the pair of models on the

1407 corresponding x and y axes. Overlaps between the vabCPM (saCPM) with the other models are

1408 illustrated in the column (row) bounded in the red (black) of each plot. Axes labels also reflect

1409 the FC-Task pair used for training the task-specific model.

1410

71

1411   Figure 8-2. Percentage of edge overlap for negative network edges between each pair of models.

1412   The value within each cell indicates the percentage of overlap between the pair of models on the

1413   corresponding x and y axes. Overlaps between the vabCPM (saCPM) with the other models are

1414   illustrated in the column (row) bounded in the red (black) of each plot. Axes labels also reflect

1415   the FC-Task pair used for training the task-specific model.

1416

1417   Figure 8-3. Percentage of edge overlap between negative network (y-axis) and positive network

1418   (x-axis) edges. The value within each cell indicates the percentage of overlap between the pair of

1419   models on the corresponding x and y axes. Overlaps between the vabCPM (saCPM) with the

1420   other models are illustrated in the column (row) bounded in the red (black) of each plot. Axes

1421   labels also reflect the FC-Task pair used for training the task-specific model.

1422

1423   Figure 8-4. Percentage of edge overlap between positive network (y-axis) and negative network

1424   (x-axis) edges. The value within each cell indicates the percentage of overlap between the pair of

1425   models on the corresponding x and y axes. Overlaps between the vabCPM (saCPM) with the

1426   other models are illustrated in the column (row) bounded in the red (black) of each plot. Axes

1427   labels also reflect the FC-Task pair used for training the task-specific model.

1428

1429 **Extended Data**

1430 Table 1-1. Detailed protocol from the full study from which the present data derives.
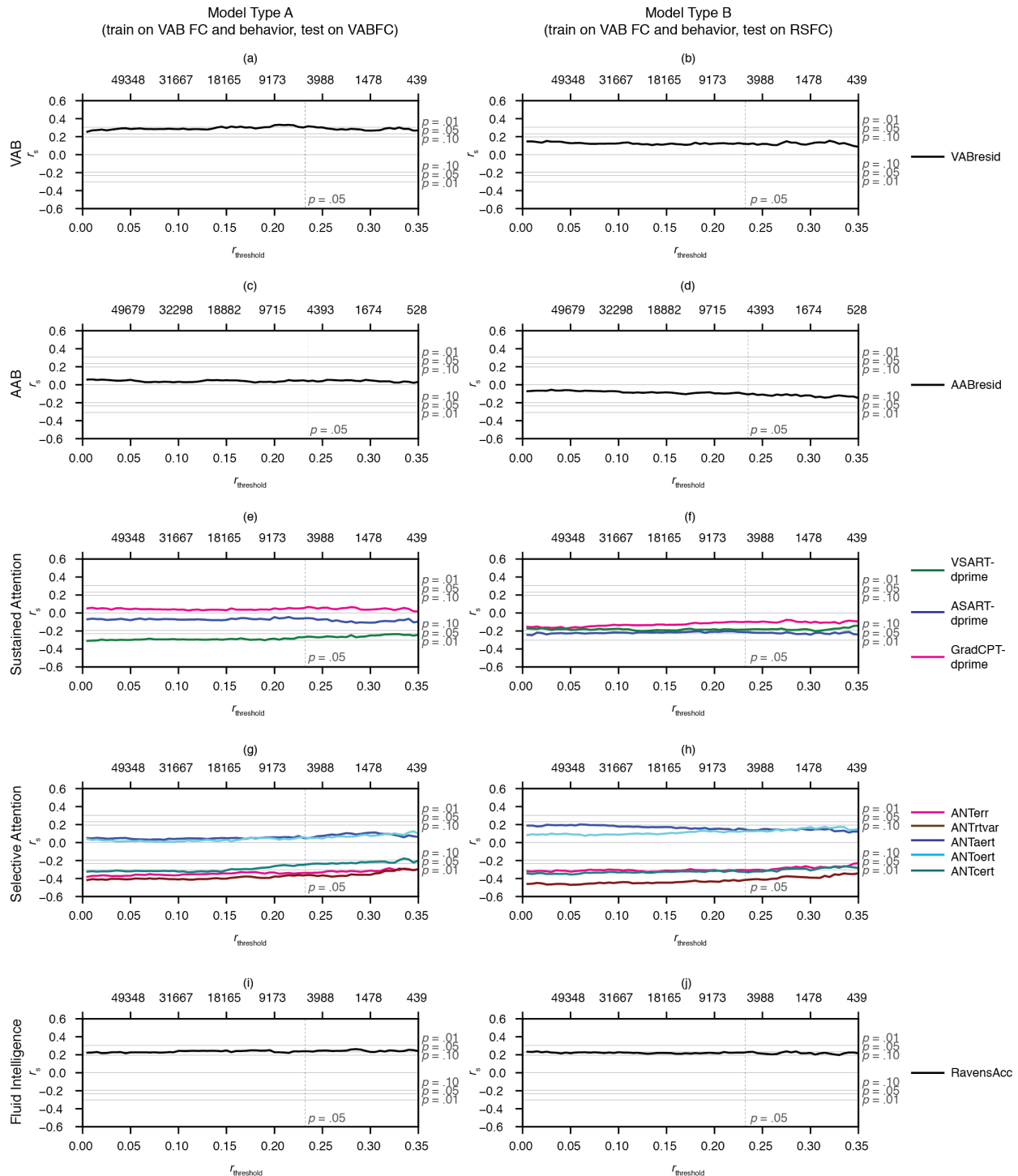
Session	Tasks/ Questionnaires	Session Description	Session Dur (hr)
1	Visual Attentional Blink (VAB) task	Participants were briefed on the study protocol in the first session and completed a target-probe Attentional Blink (AB) task to obtain a measure of baseline performance. Participants were only eligible to continue with the subsequent sessions if they obtained an average of 75% and above for target discrimination accuracy in the first session. Participants were not informed about their performance until the end of all experimental sessions.	1
2	Visual AB and surprise-induced blindness (SiB) task (in-scanner)	Participants had to return to the laboratory for the second session 3 to 14 days after the first session. The second session consisted of a 1.5 hr long fMRI scan. Task order was fixed across participants. No time limit was imposed on any of the questionnaires so participants could complete them at their own pace. All questionnaires were administered online using Qualtrics (Qualtrics, 2005).	2.5
	Short-Sleep Questionnaire		
	Visual Sustained Attention to Response task (12 mins)		
	Attentional Network Task (30 mins)		
	Theories of Intelligence Questionnaire		
3	Gradual-onset continuous Performance Task (15 mins)	The third session took place the day after the second session. Task order for the first 3 tasks was counterbalanced	2

73

|			
	Auditory Sustained Attention to Response task (12 mins)	across participants.	
	Auditory AB and Surprise-induced deafness (SiD) task		
	Visual AB task		
	Visual AB task with colour-salient training		
4	Visual AB and SiB task	The fourth session took place the day after the third session.	2
	Visual Sustained Attention to Response task (12 mins)	The Raven's Progressive Matrices task was an adapted version of the actual task that only	
	Attentional Network Task (30 mins)	consisted of 9 questions with no time limit given. Task order was fixed across participants.	
	Adult ADHD Self-Report Scale Questionnaire		
	Online Dimensional Change Card Sorting (DCCS) task		
	Raven's Progressive Matrices		
	Loss Aversion task		
5	Gradual-onset continuous Performance Task (15 mins)	The fifth session took place the day after the fourth session.	2
	Auditory Sustained Attention to Response task (12 mins)	Decision-making tasks included a cups task and an explore-exploit task. Task order for the first three computerized tasks and questionnaires were counterbalanced and	
	Auditory AB and Surprise-	randomized across participants.	

74

	induced deafness (SiD) task		
	Media-Multitasking Video Game Questionnaire		
	Personality Inventory for DSM-5 for adults		
	Wender Utah Rating Scale		
	Musical background and experience questionnaire		
	Decision-making tasks		
	Demographic Questionnaire		
6	Visual AB and surprise-induced blindness (SiB) task (in-scanner)	Session 6 was held between 5 to 14 days from the second session and consisted of a 1.5 hr long fMRI scan that used a protocol identical to that of the first in-scanner session so as to investigate test-retest reliability. Participants were encouraged to take breaks between experimental blocks and between tasks to alleviate fatigue.	1.5

1431

1432 Figure 6-1. Behavioral predictions from CPMs. Values indicate r_s and uncorrected, two-tailed p-

1433 values from Spearman's partial rank correlation, computed between predicted and observed

1434 behavioral scores, controlled for motion. The p-value corresponding to each r_s was found by

1435 transforming the correlation coefficients to Student's t values by the partialcorr.m function in

1436 (*MATLAB*, 2014). Degrees of freedom for these tests were 66 for Models A and C, and 61 for

1437 Models B and D. (For AABresid, these *d.f.* values were 2 lower.) Note that all task scores had

1438 been re-oriented so that larger values indicate better task performance.

Task domain	Train / Test / Task	Model A VABFC-VABresid VABFC-Task		Model B VABFC-VABresid RSFC-Task		Model C VABFC-Task VABFC-Task		Model D RSFC-Task RSFC-Task	
		r_s	p	r_s	p	r_s	p	r_s	p
Attentional Blink	VABresid	0.308	0.011*	0.123	0.338	0.308	0.011*	0.148	0.228
	AABresid	0.04	0.748	-0.107	0.411	0.135	0.279	-0.053	0.672
Sustained Attention	VSARTdprime	-0.268	0.027*	-0.19	0.135	0.245	0.044*	0.062	0.617
	ASARTdprime	-0.062	0.617	-0.212	0.096	-0.021	0.866	0.201	0.1
	GradCPTdprime	0.058	0.637	-0.097	0.451	-0.265	0.029*	0.226	0.063
Selective Attention	ANTerr	-0.33	0.006*	-0.308	0.014*	0.346	0.004*	0.14	0.256
	ANTrtvar	-0.36	0.003*	-0.414	0.001*	0.24	0.049*	0.232	0.057
	ANTaert	0.051	0.682	0.141	0.269	0.033	0.787	-0.061	0.619
	ANToert	0.063	0.609	0.128	0.318	0.124	0.313	0.032	0.793
	ANTcert	-0.252	0.038*	-0.333	0.008*	0.032	0.798	0.262	0.031*
Fluid Intelligence	RavensAcc	0.245	0.044*	0.224	0.077	-0.125	0.31	0.374	0.002*

1439

1440

Figure 6-2. CPM predictions for models trained with VAB functional connectivity and behavioral data (Model types A and B) across edge selection thresholds. Within each subplot, the

77

1443   y-axis represents Spearman's rank correlation values, r_s, computed between predicted and

1444   observed task performance, controlled for motion. Horizontal gray lines indicate the

1445   corresponding p = .01, .05, .10, .10, .05, .01 (top to bottom) uncorrected levels of significance

1446   from standard r-to-p conversions, $d.f.$ = 71 (69 for AAB). The x-axis represents edge selection

1447   thresholds, $r_{threshold}$. The vertical gray line indicates the $r_{threshold}$ at the p = .05 level of

1448   significance, $d.f.$ = 70 (68 for AAB) due to one left-out participant during training. X-axis labels

1449   at the top of each plot indicate the average number of edges selected across all leave-one-out

1450   iterations at the corresponding $r_{threshold}$ on the bottom x-axis.
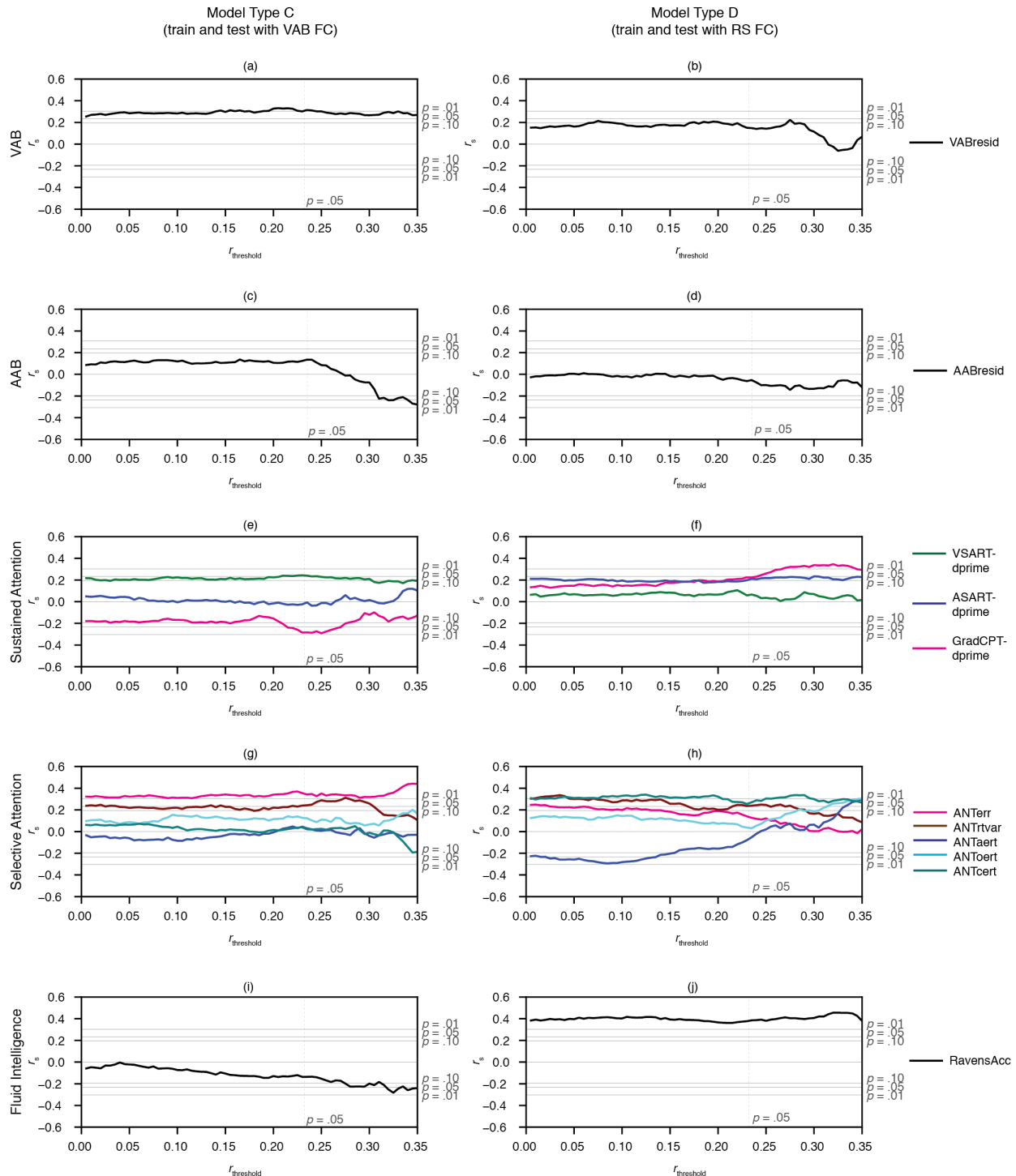
1451

1452   Figure 6-3. CPM predictions for models trained from task-specific behavioral data (Model types

1453   C and D) across edge selection thresholds. Within each subplot, the y-axis represents Spearman's

79

1454   rank correlation values, r_s, computed between predicted and observed task performance,

1455   controlled for motion. Horizontal gray lines indicate the corresponding p = .01, .05, .10, .10, .05,

1456   .01 (top to bottom) uncorrected levels of significance from standard r-to-p conversions, $d.f.$ = 71

1457   (69 for AAB). The x-axis represents edge selection thresholds, $r_{threshold}$. The vertical gray line

1458   indicates the $r_{threshold}$ at the p = .05 level of significance, $d.f.$ = 70 (68 for AAB) due to one left-

1459   out participant during training. X-axis labels at the top of each plot indicate the average number

1460   of edges selected across all leave-one-out iterations at the corresponding $r_{threshold}$ on the bottom x-
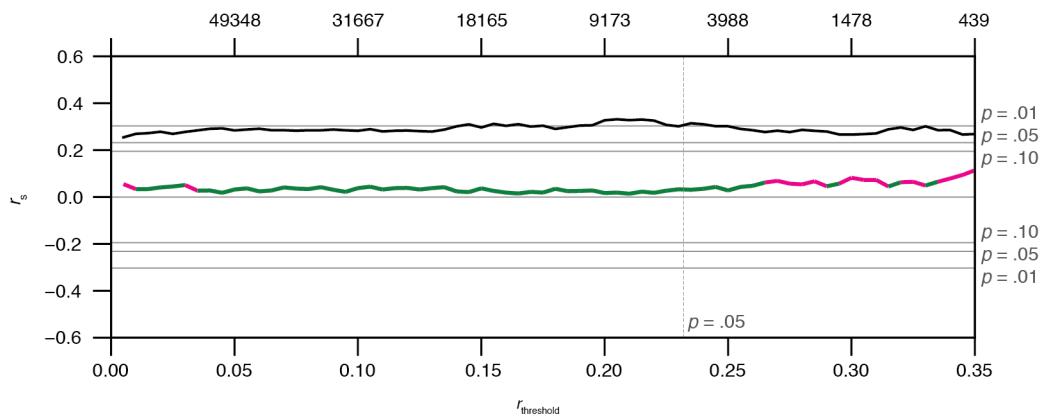
1461   axis.

1462

1463

1464   Figure 6-4. Permutation results of predicting VABresid data from VAB FC information, using

1465   the vabCPM (Model type A). The black line indicates Spearman's rank correlation values (r_s)

1466   computed between predicted and observed task performance, controlled for motion. Horizontal

1467   gray lines indicate the corresponding p = .01, .05, .10, .10, .05, .01 (top to bottom) uncorrected

1468   levels of significance from standard r-to-p conversions, based on N = 73. Green sections indicate

1469 p < .05 level of significance from permutation testing. Magenta sections indicate p ≥ . 05 level

1470   of significance from permutation testing. Our analysis demonstrates a high level of consistency

80

1471   in the significance of r_s values between using standard r-to-p conversions (black line) and using

1472   permutation testing (green/magenta line) for the majority of edge selection thresholds.

1473

1474   Figure 7-1. Results of applying the saCPM model to data in the present study. Values indicate r_s

1475   and uncorrected, two-tailed p-values from Spearman's rank correlation, computed between

1476   predicted and observed behavioral scores. The p-value corresponding to each r_s was found using

1477   standard r-to-p conversions, with $d.f. = 71$ (69 for AABresid). All task scores had been re-coded

1478   so that larger values indicate better task performance.

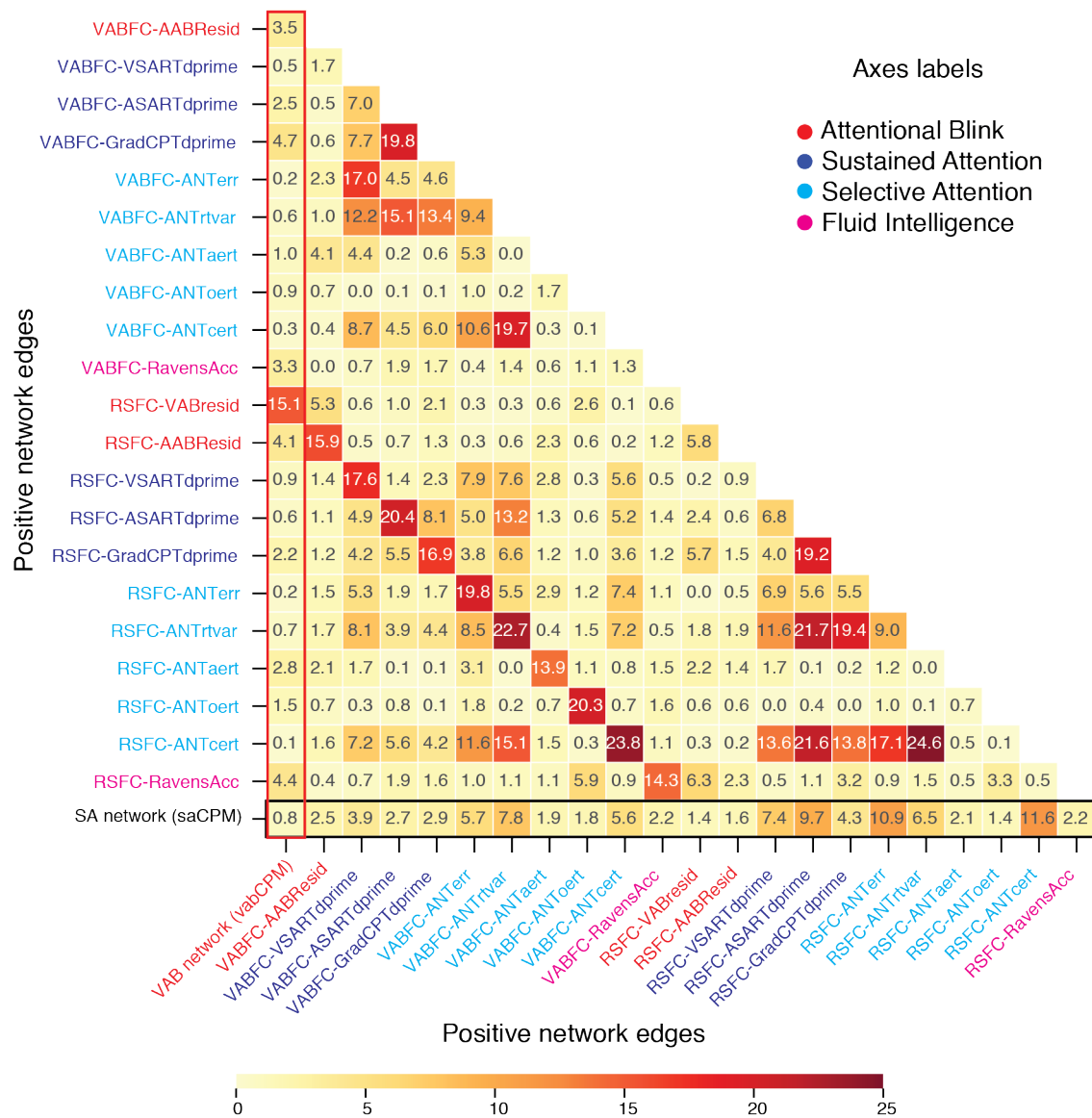| Task domain	Task	saCPM (VABFC)		saCPM (RSFC)	
		r_s	p	r_s	p
Attention Blink	VABresid	-0.235	0.045*	-0.155	0.191
	AABresid	0.049	0.684	-0.132	0.271
Sustained Attention	VSARTdprime	0.278	0.018*	0.271	0.021*
	ASARTdprime	0.117	0.323	0.290	0.013*
	GradCPTdprime	0.027	0.822	0.086	0.469
Selective Attention	ANTerr	0.322	0.005*	0.156	0.189
	ANTrtvar	0.329	0.005*	0.270	0.021*
	ANTaert	-0.057	0.629	-0.099	0.405
	ANToert	-0.101	0.397	-0.155	0.190
	ANTcert	0.224	0.057	0.384	0.001*
Fluid Intelligence	RavensAcc	-0.059	0.620	-0.229	0.052

1479

1480

1481 Figure 8-1. Percentage of edge overlap for positive network edges between each pair of models.

1482 The value within each cell indicates the percentage of overlap between the pair of models on the

1483 corresponding x and y axes. Overlaps between the vabCPM (saCPM) with the other models are

1484 illustrated in the column (row) bounded in the red (black) of each plot. Axes labels also reflect

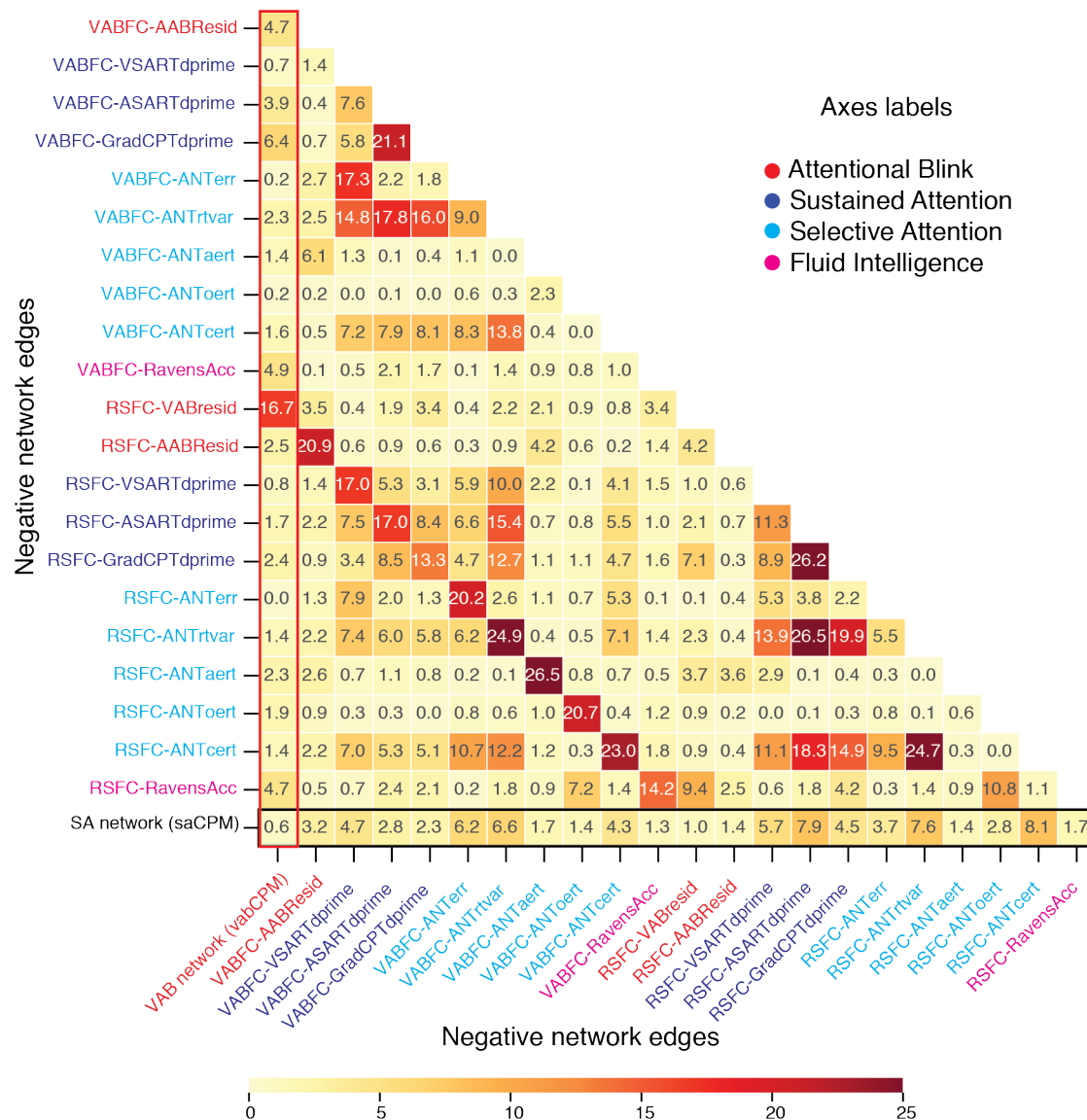1485 the FC-Task pair used for training the task-specific model.

1486

Figure 8-2. Percentage of edge overlap for negative network edges between each pair of models. The value within each cell indicates the percentage of overlap between the pair of models on the corresponding x and y axes. Overlaps between the vabCPM (saCPM) with the other models are illustrated in the column (row) bounded in the red (black) of each plot. Axes labels also reflect the FC-Task pair used for training the task-specific model.
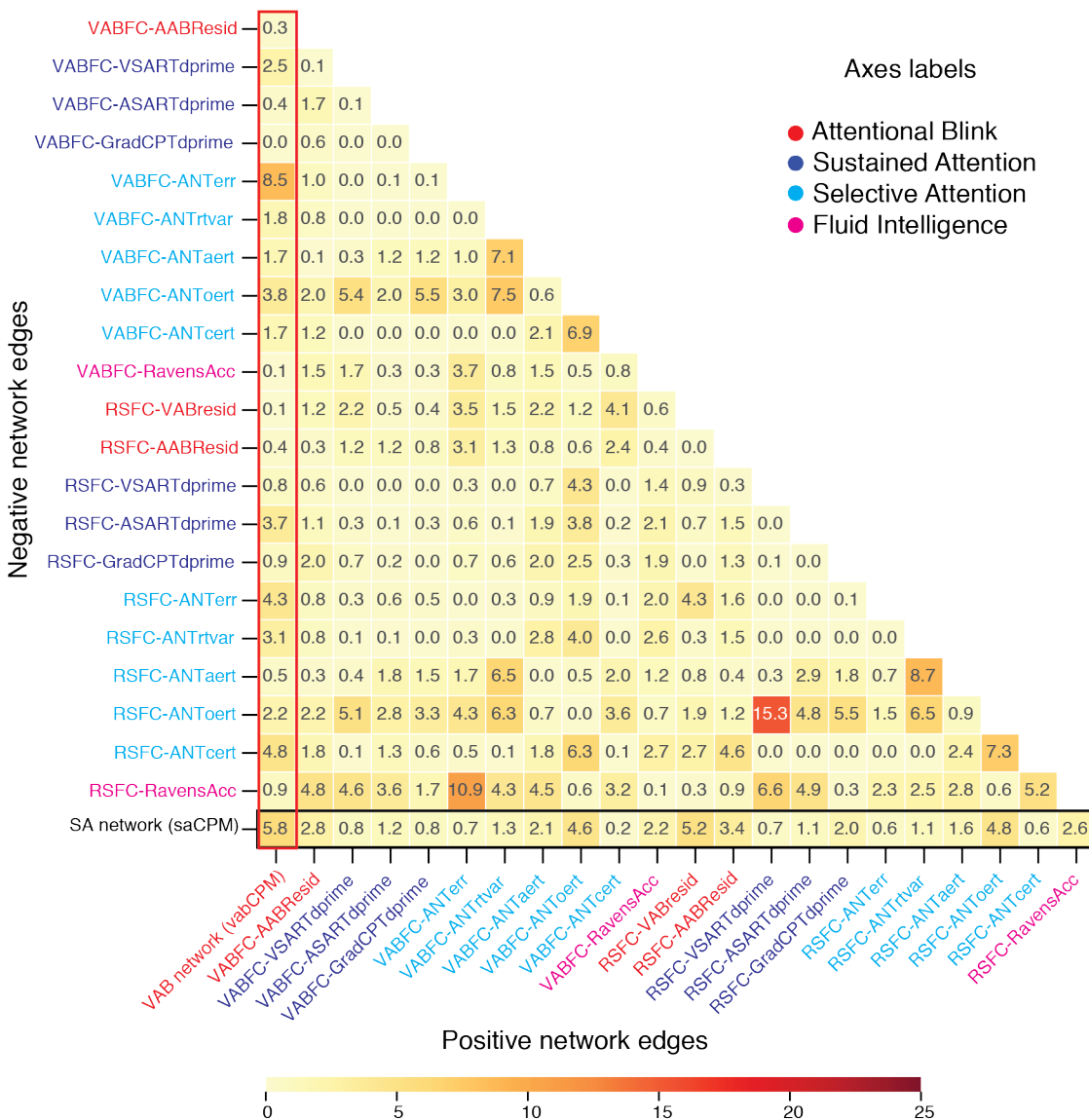
Figure 8-3. Percentage of edge overlap between negative network (y-axis) and positive network (x-axis) edges. The value within each cell indicates the percentage of overlap between the pair of models on the corresponding x and y axes. Overlaps between the vabCPM (saCPM) with the other models are illustrated in the column (row) bounded in the red (black) of each plot. Axes labels also reflect the FC-Task pair used for training the task-specific model.
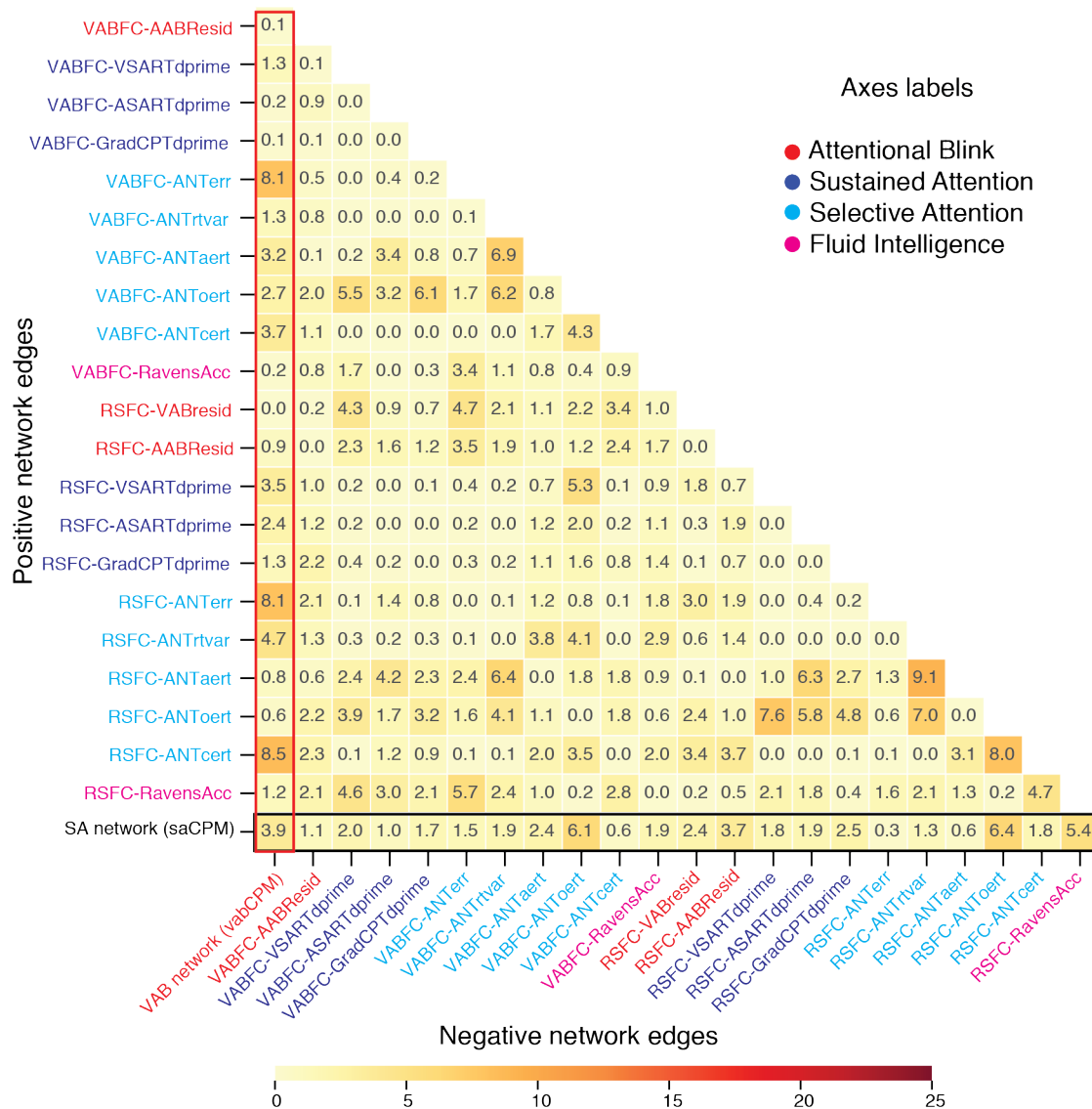
1501

Figure 8-4. Percentage of edge overlap between positive network (y-axis) and negative network (x-axis) edges. The value within each cell indicates the percentage of overlap between the pair of models on the corresponding x and y axes. Overlaps between the vabCPM (saCPM) with the other models are illustrated in the column (row) bounded in the red (black) of each plot. Axes labels also reflect the FC-Task pair used for training the task-specific model.

1507